Nano- and Micro-sized Molecularly Imprinted Polymer Particles on Solid Surfaces

Kamra, Tripta

2015

Nano- and Micro-sized Molecularly Imprinted Polymer Particles on Solid Surfaces

Tripta Kamra

LUND
UNIVERSITY

DOCTORAL DISSERTATION

by due permission of the Faculty of Science, Lund University, Sweden.
To be defended in Lecture Hall F (K404) at the Department of Physics.
Monday 14 September 2015, at 10:15.

Faculty opponent:
Dr. Mohamed M. Chehimi
Department of Chemistry
University Paris Diderot, Paris

Organization
LUND UNIVERSITY
Division of Synchrotron Radiation Research,
Department of Physics, Box 118, 221 00 Lund
Author: Tripta Kamra

Document name
DOCTORAL DISSERTATION
Date of issue
August 6, 2015
Sponsoring organization

Title and subtitle

Nano- and Micro-sized Molecularly Imprinted Polymer Particles on Solid Surfaces

Abstract

Molecularly imprinted polymers (MIPs) are artificial receptors made by imprinting template molecules in a polymer matrix followed by their removal through washing to obtain a specific and selective template cavities. This property of the MIPs have made them a very efficient material for diverse applications such as chromatography, purification, drug sensing, etc. Recently, zero-dimensional polymer materials, in the present case molecularly imprinted polymer nanoparticles (MIP nanoparticles), have been used widely for the fabrication of various functional materials. The large surface area of MIP nanoparticles leads to better and efficient template binding. Nanoparticles synthesized with a thin and uniform shell (core-shell MIP nanoparticles) have provided additional functional groups (amine, thiols) that can be advantageous for different analytical applications.In this thesis, the immobilization of both MIP and MIP core-shell nanoparticles on solid surfaces and the application of Surface enhanced Raman scattering (SERS) on MIP-modified surfaces for the detection of an analyte (propranolol and nicotine) have been studied. In the first part of the thesis different covalent and electrostatic approaches for the immobilization of imprinted polymer nanoparticles on glass, silicon, and Au wafers are reported. The covalent approaches comprises photoconjugation, epoxide ring opening reactions, and carbodiimide chemistry. In the electrostatic approach a polymer interlayer has been used. The surfaces with immobilized particles are characterized using different surface analytical techniques. The morphology and surface property of the particles' surfaces are reported using scanning electron microscopy (SEM), atomic force microscopy (AFM), fluorescence microscopy, and water contact angle measurements. Further, the chemical analysis of the surfaces using x-ray photoelectron spectroscopy (XPS) confirms the functionalization of the solid surfaces before and after MIP immobilization. Finally, the template binding property (selectivity and specificity) of the immobilized particles are reported using autoradiography measurements. In the second part of the thesis I report the different surface morphologies for of the SERS detection of propranolol and nicotine sensing in imprinted nano- and micro sized polymer spheres. Nicotine-imprinted MIP spheres were immobilized on a Au wafer using surface thiols. After the confirmation of stable and dense particle attachment using SEM, the Au surfaces were made SERS active either using Au colloids or replacing Au with Raman-active Klarite surfaces. The propranolol-imprinted nanoparticles are attached to Klarite using a photoconjugation approach. Using SERS as the detection method I analyzed the binding capacity of the polymer sphere-coated transducer surface. The MIPs exhibit good specificity and selectivity in a complex biological sample.

Key words: Molecularly imprinted polymers, glass, gold,, epoxide, thiols, carbodiimide chemistry, scanning electron microscopy, X-ray photoelectron spectroscopy, surface enhanced Raman spectroscopy, propranolol, nicotine.

Classification system and/or index terms (if any)

Supplementary bibliographical information
Language: English

ISSN and key title

ISBN:
978-91-7623-424-2 (print)
978-91-7623-425-9 (pdf)

Recipient's notes

Number of pages 227
Price

Security classification

Signature Tripta Kamra Date 2015-08-06

Nano- and Micro-sized Molecularly Imprinted Polymer Particles on Solid Surfaces

Tripta Kamra

LUND
UNIVERSITY

Division of Synchrotron Radiation Research
Department of Physics
and
Pure and Applied Biochemistry
Department of Chemistry
Lund University

Front cover:

Colored scanning electron microscopic image of molecularly imprinted polymer microspheres embedded inside lithographically patterned Klarite wells.

Division of Synchrotron Radiation Research
Department of Physics
Lund University
Faculty and Department
ISBN: 978-91-7623-424-2 (print)
978-91-7623-425-9 (pdf)

Printed in Sweden by Media-Tryck, Lund University
Lund 2015

Dedicated to my loving parents and brother especially to my mother
Love u momma…….

Abstract

Molecularly imprinted polymers (MIPs) are artificial receptors made by imprinting template molecules in a polymer matrix followed by their removal through washing to obtain a specific and selective template cavities. This property of the MIPs have made them a very efficient material for diverse applications such as chromatography, purification, drug sensing, etc. Recently, zero-dimensional polymer materials, in the present case molecularly imprinted polymer nanoparticles (MIP nanoparticles), have been used widely for the fabrication of various functional materials. The large surface area of MIP nanoparticles leads to better and efficient template binding. Nanoparticles synthesized with a thin and uniform shell (core-shell MIP nanoparticles) have provided additional functional groups (amine, thiols) that can be advantageous for different analytical applications.

In this thesis, the immobilization of both MIP and MIP core-shell nanoparticles on solid surfaces and the application of Surface-enhanced Raman scattering (SERS) on MIP-modified surfaces for the detection of an analyte (propranolol and nicotine) have been studied. In the first part of the thesis different covalent and electrostatic approaches for the immobilization of imprinted polymer nanoparticles on glass, silicon, and Au wafers are reported. The covalent approaches comprises photoconjugation, epoxide ring opening reactions, and carbodiimide chemistry. In the electrostatic approach a polymer interlayer has been used. The surfaces with immobilized particles are characterized using different surface analytical techniques. The morphology and surface property of the particles' surfaces are reported using scanning electron microscopy (SEM), atomic force microscopy (AFM), fluorescence microscopy, and water contact angle measurements. Further, the chemical analysis of the surfaces using x-ray photoelectron spectroscopy (XPS) confirms the functionalization of the solid surfaces before and after MIP immobilization. Finally, the template binding property (selectivity and specificity) of the immobilized particles are reported using autoradiography measurements.

In the second part of the thesis I report the different surface morphologies for of the SERS detection of propranolol and nicotine sensing in imprinted nano- and micro sized polymer spheres. Nicotine-imprinted MIP spheres were immobilized on a Au

wafer using surface thiols. After the confirmation of stable and dense particle attachment using SEM, the Au surfaces were made SERS active either using Au colloids or replacing Au with Raman-active Klarite surfaces. The propranolol-imprinted nanoparticles are attached to Klarite using a photoconjugation approach. Using SERS as the detection method I analyzed the binding capacity of the polymer sphere-coated transducer surface. The MIPs exhibit good specificity and selectivity in a complex biological sample.

Popular Science Summary

Nanoscience and nanotechnology have existed in this world before scientists actually coined the terms. Nature around us and human beings themselves are all made of nanomaterials (1-100 nm), such as DNA, proteins, liposomes, and enzymes. These building blocks possess molecular recognition properties, resulting in their self-assembly to form various two- and three-dimensional nanostructured materials useful in the field of science and technology. Scientists from different disciplines, including physics, chemistry, biology, and material science, use these nanostructured materials for advanced applications in medicine, energy, etc.

The detection of drugs in therapeutic applications requires selective molecular interaction with the target material. Thus, researchers have designed biosensors for detecting and sensing molecules in biological materials, e.g., glucose biosensors, which are quite important for sensing the glucose levels in the body. Biosensors can work when the biomolecules or the recognition materials are perfectly integrated with the transducer surface. These transducer surfaces are a very important element of the sensor fabrication as they convert the biological recognition event into a detectable signal.

The basic recognition mechanism, the analyte binding by the immobilized biomolecule, depends on the famous **"lock and key method"** first reported by the Nobel-Prize laureate Emil Fischer in 1894. The interaction between the lock and key should be reversible and stable to ease the operation and for reuse of the chemical sensor. Due to the poor stability of the biological recognition material in different physical and chemical environments, biosensors may give false readings. Further, the binding event is sometimes irreversible, which makes these biosensors suitable for only one-time use, making them more expensive.

To solve this problem, the biomaterials may be replaced by "artificial receptors" or "plastic antibodies," referred to as molecularly imprinted polymers (MIPs). These polymer materials are synthesized in the presence of template molecules. After the polymerization, the template molecules are extracted, leaving behind "cavities" or "memory sites" with high selectivity and specificity for the template. The feature of

molecular “memory” imprinted into the polymers enables them to selectively rebind the templates multiple times, which is similar to the “lock and key mechanism.” The template molecules can be any biomolecule, such as antibodies, enzymes, nucleic acids, microorganisms (bacteria, viruses) or drugs. This makes the MIPs suitable for the detection of drugs or for food-based sensing application studies with their ease of quality control, easy handling and cost effectiveness.

The most important criteria to develop a chemical sensor based on MIPs is their stable and uniform integration with the transducer surface. Therefore, this research investigates different immobilization approaches of spherical and hydrophobic MIP particles on a solid transducer surface. Different covalent and electrostatic chemistries have been studied for the dense, uniform and stable attachment of polymer spheres to chemically functionalized inorganic supports, such as glass, silica, and gold wafers. A detailed investigation of the MIP-integrated surfaces using different surface analytical techniques demonstrated the presence of polymer spheres on the transducer surface with stability in both physical and chemical environments. The MIP surfaces retain their characteristic template-binding property after immobilization on the transducer surface, thus making them suitable for sensing applications.

Ease of fabrication, low cost, sensitivity, selectivity and stability have made MIP sensors popular in physical, chemical, and biological sensing applications, e.g., the detection of various poisonous materials in the environment, food, and humans. Optical-based sensing systems are well known due to their ease, low cost and sensitivity. In principle, MIP-based optical sensors require fluorescent labels to detect the analyte binding, which makes the sensing process long and complicated. In my research, I have developed an easy, reproducible and label-free optical sensor that can be used for direct real-time measurement of analytes at different concentrations. MIP spheres imprinted against two model compounds, nicotine and propranolol, were used. Nicotine is found in cigarettes, and propranolol is a drug used to control anxiety and depression. MIP-based optical sensors were developed by the covalent immobilization of MIP spheres on an optically active transducer surface. The obtained results clearly demonstrated that the MIP surfaces are selective and specific towards analyte (propranolol and nicotine) sensing, even in the biological samples.

The reported immobilization and sensing approach can be used in biomedicine to perform both *in vivo* and *in vitro* investigations of molecules and organisms that cause health hazards. Further, these optical sensors have a wide range of

applications, such as the identification of chemical warfare agents and of different dyes useful in the defense and art industries. Different immobilization approaches reported in this thesis can also be used to attach large-sized soft polymer spheres onto solid substrates for numerous material-based applications.

Abbreviations

0D, 1D, 2D, 3D	Zero-, one-, two-, and three- dimensional
4-MBA	4-mercaptobenzoic acid
ANOP	1-amino-3-(naphthalen-1-yloxy) propan-2-ol
APTES	(3-aminopropyl) triethoxysilane
AIBN	Azobisisobutyronitrile
AFM	Atomic force microscopy
BPA	Bisphenol A
CDB	Cumyl dithiobenzoate
CRP	Controlled free radical polymerization
DVB	Divinylbenzene
EDC	1-Ethyl-3-(3-dimethylaminopropyl)carbodiimide
EGDMA	Ethylene glycol dimethylacrlyate
GE	Grazing emission
GPTMS	(3-glycidooxypropyl) trimethoxysilane
MAA	Metharylic acid
MBA	*N*,*N*-methylene-bis-acrylamide
MIP	Molecularly imprinted polymer
MUA	11-mercaptoundecanoic acid
NE	Normal emission
NHS	N-Hydroxysuccinimide
NIPAM	*N*-isopropylacrylamide
NIP	Non-imprinted polymer
PAAm	Polyallylamine
PFPA	Perfluorophenyl azide
SAM	Self-assembled monolayer
SEM	Scanning electron microscope
SERS	Surface-enhanced Raman spectroscopy
SPR	Surface plasmon resonance
STM	Scanning tunneling microscope
TNT	2, 4, 6- trinitrotoluene

TRIM	Trimethylpropane trimethacrylate
XPS	X-ray photoelectron spectroscopy
^{3}H	Tritium

List of Publications

This thesis is based on the following papers. They are referred to in the text by their Roman numerals.

I. Controlled Short-Linkage Assembly of Functional Nano-Objects.

Shilpi Chaudhary, ***Tripta Kamra****, Khan Mohammad Ahsan Uddin, Olesia Snezhkova, H. Surangi N. Jayawardena, Mingdi Yan, Lars Montelius, Joachim Schnadt, and Lei Ye,* Applied Surface Science 300, 22–28 (2014).

II. Covalent Immobilization of Molecularly Imprinted Polymer Nanoparticles using an Epoxy Silane.

Tripta Kamra*, Shilpi Chaudhary, Changgang Xu, Niclas Johansson, Lars Montelius, Joachim Schnadt, and Lei Ye,* Journal of Colloid and Interface Science 445, 277–284 (2015).

III. Covalent Immobilization of Molecularly Imprinted Polymer Nanoparticles on Gold Surface using Carbodiimide Coupling for Chemical Sensing.

Tripta Kamra*, Shilpi Chaudhary, Changaang Xu, Lars Montelius, Joachim Schnadt, and Lei Ye* (Submitted to Journal of Colloid and Interface science).

IV. Electrostatic attachment of Molecularly Imprinted Nanoparticle on Polymer-Functionalized Solid Surface.

Tripta Kamra*, Changgang Xu, Lars Montelius, Joachim Schnadt, and Lei Ye* (In manuscript).

V. Implementation of Molecularly Imprinted Polymer Beads for Surface Enhanced Raman Detection.

Tripta Kamra*, Tongchang Zhou, Lars Montelius, Joachim Schnadt, and Lei Ye*, Analytical Chemistry 87, 5056-5061 (2015).

VI. Photoconjugation of Molecularly Imprinted Polymer for Surface Enhanced Raman Detection of Propranolol.

Tripta Kamra*, Changgang Xu, Lars Montelius, Joachim Schnadt, Samurdhi A. Wijesundera, Mingdi Yan, and Lei Ye* (In manuscript).

Papers that I have contributed to that are not included in the thesis:

I. Bacterial Imprinting at Pickering Emulsion Interfaces.

Xiantao Shen, Johan Svensson Bonde, ***Tripta Kamra****, Leif Bülow, Jack C Leo, Dirk Linke, and Lei Ye*, Angewandte Chemie 53,10687-10690 (2014).

II. Fluorescent Boronic Acid Polymer Grafted on Silica Particles for Affinity Separation of Saccharides.

Zhifeng Xu, Khan Mohammad Ahsan Uddin, ***Tripta Kamra****, Joachim Schnadt, and Lei Ye*, ACS applied materials & interfaces 6, 1406-1414 (2015).

III. Preparation of Protein Imprinted Polymer Beads by Pickering Emulsion Polymerization.

Tongchang Zhou, Ka Zhang, ***Tripta Kamra****, Leif Bülow, and Lei Ye,* Journal of Materials Chemistry B 3, 1254-1260 (2015).

IV. Electrospray Deposition of Gold-Loaded Block Copolymer Reverse Micelles onto a Clean TiO_2.

Ashley Head, Shilpi Chaudhary, Maria Messing, Florent Bacque, Niclas Johansson, Olesia Snezhkova, ***Tripta Kamra****, Jesper Andersen, and Joachim Schnadt* (Submitted to Nanotechnology).

V. Synchrotron-Based XPS Studies of Adsorption of (3-aminopropyl)triethoxysilane on Rutile TiO_2(110) in UHV and at Ambient Pressure.

Shilpi Chaudhary, Rocío Sánchez-de-Armas, Ashley R. Head, Niclas Johansson, Olesia Snezhkova, ***Tripta Kamra****, Lei Ye, Lars Montelius, Fabrice Bournel, François Rochet, Jean-Jacques Gallet, Barbara Brena, and Joachim Schnadt* (In manuscript).

My contributions to the papers

I. I participated in the experiments and XPS data analysis and took part in the discussion of results. I assisted Shilpi Chaudhary in writing the first draft of the thesis.

II. I planned and performed the experiments except for the synthesis of the molecularly imprinted polymer particles. I was the main responsible for the surface characterization experiments and analysis except for the XPS measurements. I wrote the manuscript together with Shilpi Chaudhary.

III. I planned and performed all experiments except for the synthesis of the molecularly imprinted polymer particles. I was the main responsible for the surface characterization experiments and their analysis except for the XPS measurements. I wrote the manuscript together with Shilpi Chaudhary.

IV. I planned and performed all experiments except for the synthesis of the molecularly imprinted polymer particles. I was the main responsible for all experiments and data analysis and wrote the manuscript.

V. I planned and performed all experiments except for the synthesis of the molecularly imprinted polymer particles. I was the main responsible for all experiments and data analysis and wrote the manuscript.

VI. I planned and performed all experiments except for the synthesis of the molecularly imprinted polymer particles and other molecules. I was the main responsible for all experiments and data analysis and wrote the manuscript.

Contents

1. Introduction

1.1 Research background and motivation

Nanoscience and nanotechnology offer important tools required for the development of novel functional materials and devices for different applications.[1-6] Functional nanomaterials and devices are produced using either the so-called "top-down" or "bottom-up" approaches. As seen in Figure 1.1, the ***top-down approach*** involves the breaking down of bulk materials into nano-sized structures or particles. An example of such a technique is the ball milling, lithographic patterning techniques, e.g., nanoimprint lithography for the fabrication of electronic devices. The other approach, called ***bottom-up***, results in less wastage of material, and strong covalent bonds hold the building blocks together. In this approach, the individual base elements (atoms) are linked together to form a subsystem (nanoparticles) that is finally self-assembled to form a functional nanomaterial (*cf.* Figure 1.1). This is the most widely used approach due to the possible tuning of the building blocks (atoms, molecules, nanoparticles, nanowires, etc.) to form organic, inorganic, or hybrid nano- or microparticle-assembled nanostructures, which are very much required in areas such as nano-sensors,[7,8] solar cells,[8,9] biomedical devices,[10] and catalysis.[11,12]

Nanostructured materials are broadly classified in terms of their dimensionality, i.e., 0D, 1D, 2D, or 3D. I have been dealing with 0D and 3D materials. In 0D, one observes all types of nanoparticles and nanoclusters with different shapes, morphologies (spheres, capsules, etc.) and compositions (metal, organic polymer, and semiconducting material). Nanoparticles have a tendency to agglomerate, and in some applications, homogenously dispersed nanoparticles are required. This problem can be circumvented by the adsorption of ionic species or polymer brushes, referred to as ***colloids***, on nanoparticle surfaces to prevent them from agglomeration. Owing to their large surface area and other superior properties (quantum size effect and better transport of molecules in three dimensions), 3D materials have attracted

considerable research interest.[13] For the development of 3D materials (nanocomposites, zeolites, nanocoils, etc.) 0D materials, such as biomolecules (proteins, amino acids, and nucleic acids), polymer colloids, or metal nanoparticles, can be self-assembled for applications such as biosensors[14,15] and optoelectronics.[16,17]

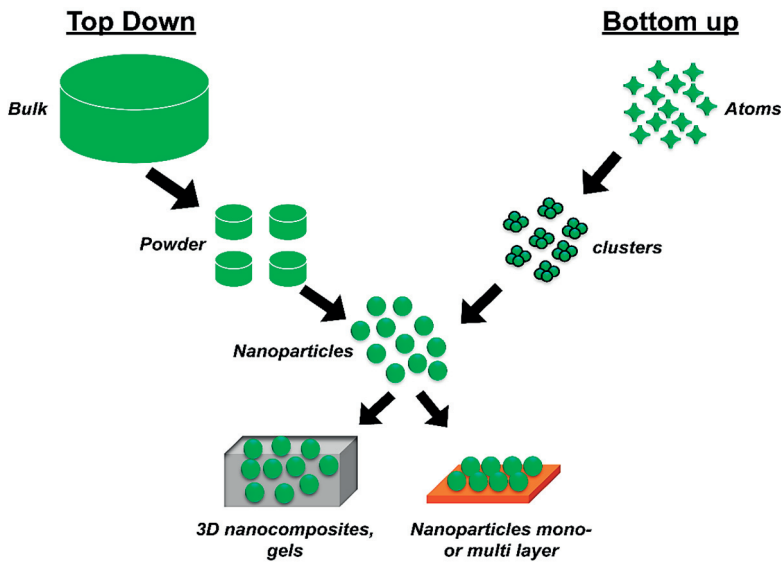

Figure 1.1 Schematic representation of the top-down and bottom-up approaches used for building nanomaterials.

Over the last few decades, an enormous amount of research and development has been performed regarding sensor technology. The detection and monitoring of different chemicals, contaminants, and microorganisms in the environment and food is important for human life. To accomplish sensitive and specific monitoring, biosensors, as well as chemical sensors, are ideal candidates due to their handy operation. A biosensor relies on the 'specific molecular recognition' property of the recognition material for the specific and selective detection of bioactive molecules, such as drugs,[18] proteins, and nucleic acids,[19] in complex samples. Figure 1.2 represents a general scheme of a biosensor design. The recognition material is interfaced with a transducer, and specific analyte binding generates a specific

change of mass, electrical energy, thermal energy or capacitance, which is converted into a signal using digital electronics. In biosensors, the recognition elements may be obtained from different biological systems, e.g., antibodies and aptamers that are particularly useful for the detection of biomacromolecules. These biological systems are, however, not particularly successful in recognizing low-molecular-weight analytes, and moreover, they have only limited stability (chemical and physical) and sensitivity in non-optimal environments.[20] Therefore, it is often necessary to switch to synthetic receptors with high stability and cost effectiveness.

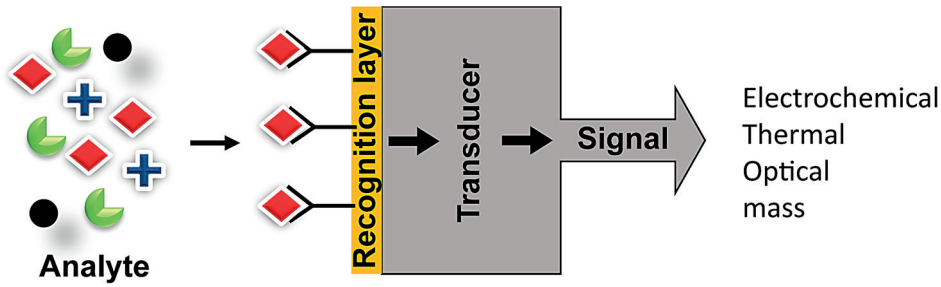

Figure 1.2. General schematic representation of chemical sensors or biosensors.

A recent development is the replacement of biological material with a particular type of synthetic polymer material, the so-called "***molecularly imprinted polymers (MIPs)***." MIPs are cross-linked polymers with predesigned molecular selectivity produced by template-guided polymerization.[21,22] They possess high mechanical and chemical stability, which provides MIP-based chemical sensors with outstanding durability. MIPs can be directly fabricated *in situ* on a transducer surface to act as a molecular recognition layer for the detection of the template or its structural analogs. A major problem associated with *in situ*-fabricated MIP sensors is, however, the inaccessibility of a large fraction of the template sites due to the layers' small surface area. With *ex situ*-prepared MIP-based sensors, this problem can be circumvented because these MIPs can be synthesized as particles with a large surface-to-volume ratio. Different types of molecularly imprinted polymer nanoparticles (MIP nanoparticles) are reported in the literature, such as magnetic nanoparticles, metal-coated nanoparticles, and fluorescent nanoparticles. In this thesis, Chapter 2 describes in detail the different imprinted polymer nanoparticles and microbeads used in my work. The polymeric spheres possess

different functionalities and were imprinted against two model compounds, propranolol and nicotine.

Combining the molecular selectivity of MIP nanoparticles with a spectroscopic transducer has been proven very powerful for the detection of organic molecules in complex samples, thanks to the synergy of selective molecular binding from the MIP and the fingerprint identification offered by the spectroscopic transducer.[23-26] Previously, MIPs have been combined with IR evanescent wave spectroscopy[27] and a surface-enhanced Raman scattering (SERS) transducer in order to detect small organic analytes. Among the different optical sensing constructs, MIP sensors using SERS detection have become the most popular,[28-31] and portable Raman instruments are now available from many commercial vendors, with which detection can be carried out directly on both solid and liquid samples.

1.2 Aim of this work

The main objective of my thesis was to design new approaches to assemble MIP nanoparticles on a transducer surface for Raman-based sensor applications. To achieve a reusable and efficient sensor, one needs a uniformly packed high-density layer of MIP particles on the transducer surface. To achieve this objective, polymer particles should be chemically attached on the solid transducer surface using different immobilization approaches.

This thesis is structured as follows: the thesis starts with the information of the MIP particles (Chapter 2), followed by the description of the experimental techniques used in this work (Chapter 3). Finally, in Chapter 4, I discuss the results of my work, and present conclusions with a future outlook in the last chapter.

In terms of the papers included in this thesis, the ***first part*** of my work (**Papers I-IV**) was to study different immobilization chemistries for the attachment of functionalized MIP spheres, either directly on the functionalized surface or using some functional linkers/spacers. I have initiated a study to understand the stable immobilization of MIP particles on solid surfaces (microscopic glass slides, silicon wafers, and Au wafers) using different interactions (covalent and electrostatic). The investigation of the morphology and surface functional groups of immobilized imprinted particles was conducted using different surface analysis tools. Finally,

template-binding experiments were performed to confirm the selectivity and specificity of the imprinted polymer-modified solid surfaces.

The ***second part*** of the thesis (**Papers V and VI**) focuses on the sensing of two addictive drugs, nicotine and propranolol, using the MIP-based optical sensors. Nicotine is a hazardous compound found in cigarettes, whereas propranolol is a famous drug used by musicians, actors, sportsmen, and public speakers for its ability to control heart palpitations and anxiety. Thus, an efficient sensor is required to detect the levels of these drugs in the biofluid. The aim of this part of the research was to extend the work performed in the first part with a focus on the application of the MIP particles' integrated surfaces for sensing nicotine and propranolol using SERS as an analytical tool. A uniformly and densely packed MIP spheres assembly on an Au wafer and SERS active Klarite was achieved using covalent immobilization. The MIP surfaces showed the selective and specific template-binding property. This information is the key for developing other MIP particles and making them SERS active using patterned substrates, for sensing other biomolecules, toxins, and drugs in biological samples.

2. Molecularly imprinted polymers

2.1 Molecular imprinting

Molecular recognition is an essential property of any biological system and plays an important role in, e.g., enzyme, antibody, and nucleic acid chemistry.[32] During the last decades, research has focused on replacing these biological receptors with an artificial material to overcome the problems of poor stability and the high cost of the biological receptors.[33-39] One such major development is ***molecular imprinting*** in synthetic polymers. Molecular imprinting is known to originate from an experiment by Russian scientist Polyakov in 1931 who prepared a silica gel by the polymerization of sodium silicate with ammonium carbonate. The silica gel was then used to selectively adsorb different solvent molecules that were added during the silica gelaton.[40] Molecular imprinting has been reported useful for the preparation of selective adsorbents for the detection of various types of drugs and biomolecules.[41]

Molecular imprinting is a polymerization technique that creates selective cavities in a polymer matrix. These cavities are complementary to the target molecule (template) present in the polymer mixture during the polymerization. Figure 2.1 shows the principle involved in molecular imprinting. In a solution of the template (imprint molecule), functional monomers copolymerize with cross-linkers. An initiator is included in the solution as well, in order to initiate the polymerization. Initially, the monomer, template, and cross-linker form a complex, and after the polymerization, the functional groups are tightly held in place with the help of cross-linking. The template molecule in the resulting molecularly imprinted polymer can be removed, leaving behind a molecular cavity that can rebind the template.[22]

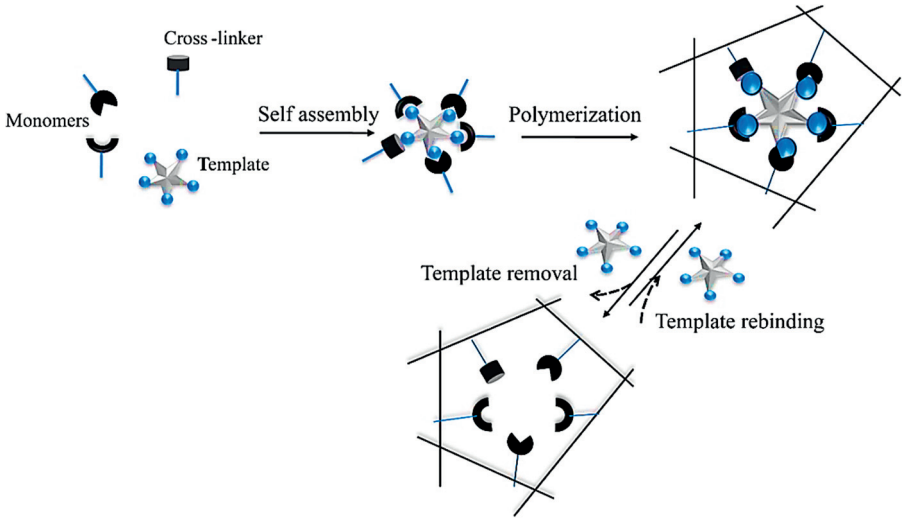

Figure 2.1 Schematic representation of the molecular imprinting.

The intermolecular interaction of the template with the MIPs can be ionic, dipole-dipole, hydrogen bonding, covalent, or non-covalent in nature. There are three different approaches for molecular imprinting. In the first approach, the monomers and the template molecule can be coupled ***covalently*** to each other, and the removal of the template is achieved by the chemical cleavage of the covalent bond. This approach can lead to stable and selective (in shape and size) binding sites.[42] In the second approach, functional monomers and the template interact via non-covalent interactions (self-assembly). This ***non-covalent imprinting*** approach was invented by Mosbach and co-workers.[22] This approach is very flexible and popular because of the broad possible choices of functional monomers, cross-linkers, and the template molecules.[43] The third is the ***semi-covalent*** imprinting approach, invented by Whitcombe and co-workers.[44] In this approach, covalent bonding is used to form a template-monomer polymer complex during polymerization, but non-covalent interactions are used for template rebinding. The development of MIPs using covalent and semi-covalent interactions proved to be very challenging. In my research, I have focused on the non-covalent imprinting approach to imprint different template molecules.[45] Figure 2.2 shows the different functional monomers, cross-linkers, initiators, and templates used to synthesize the MIP particles using the

non-covalent approach. In a particular imprinting experiment, the monomer, initiator, cross-linker, and a template molecule are mixed and polymerized. The obtained polymer is then grounded and sieved. The template is removed by washing the MIPs repeatedly by acetic acid in methanol to obtain highly selective and specific binding cavities. In the following section, I will describe the different non-covalent polymerization routes used in this thesis for the synthesis of MIP nanoparticles and microbeads in more detail.

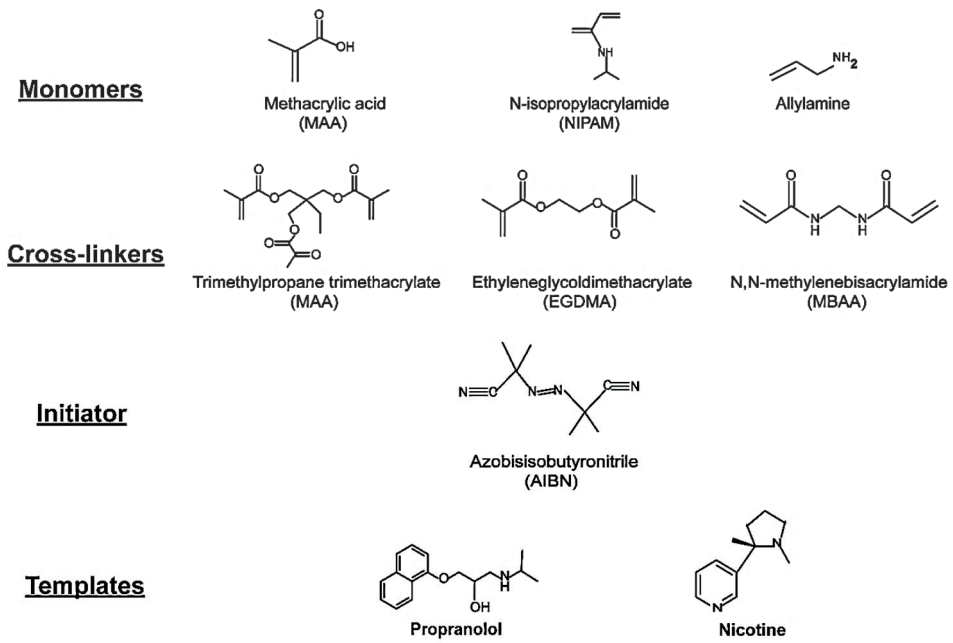

Figure 2.2. Building blocks for molecularly imprinted polymer synthesis: functional monomers, cross-linkers,[46] initiator, and template molecules used in this thesis.

2.2 Molecularly imprinted polymer nanoparticles and microbeads

In many high-performance materials, MIPs with well-defined shape and size are required. This requirement can be fulfilled by the use of MIP nanoparticles. The extraordinary large surface area of nanoparticles presents diverse opportunities to exploit the functional groups available on the MIP nanoparticles' surface. Recently, uniform imprinted nanoparticles have been prepared using self-assembly of well-defined monomers as starting materials, followed by a cross-linking reaction in a special solvent to create imprinted cavities for a specific template.[47] The methods commonly used to prepare MIP nanoparticles include emulsion polymerization, miniemulsion polymerization, microemulsion polymerization, precipitation polymerization, and surface grafting polymerization. The MIP nanoparticles reported in the literature can have different geometries and size, i.e., nanospheres, core-shell particles, and different hollow spheres. In the following sections (2.2.1-2.2.3), I describe in detail the different polymerization routes used to synthesize the MIP nanoparticles studied here in the presented work.

2.2.1 MIP nanoparticles by precipitation polymerization

MIPs are mostly prepared using bulk polymerization. The resulting polymer is then grounded and sieved into particles with sizes in the micron range for different applications. This conventional approach is simple and cost effective but often produces particles of irregular shape and size. Moreover, the grinding steps can destroy some recognition sites, which reduces the MIPs' binding capacity.[48,49] For new and advanced analytical applications, MIPs with well-controlled physical geometry and size are desirable. To produce MIPs as spherical beads with a size in the nanometer range (MIP nanoparticles), a widely used polymerization method is ***precipitation polymerization***.[50,51]

In precipitation polymerization, the monomer mixture is the same as in bulk polymerization except for the presence of a large amount of solvent, which allows the polymer chains to continuously grow and precipitate out from the solvent when

the size of the polymer becomes too large to be soluble in the solvent. The polymer beads are then recovered and washed using centrifugation and solvent exchange. No interfering reagents, such as surfactants or stabilizers, are involved in the polymerization, which makes this method suitable for a broad range of templates.

To obtain MIP beads of controlled size in the range of 100 nm to 3 μm in diameter, the ratio of the cross-linkers (DVB and TRIM) can be varied. The obtained MIP nanoparticles maintain excellent binding properties that are suitable for binding assays.[52] One of the major disadvantages with this polymerization method is that the imprint molecule needs to have high solubility in the monomer mixture because it otherwise may be lost in the reaction solvent. Therefore, the solvent plays an important role in governing the MIPs' formation by bringing all the building blocks (monomers, initiator, cross-linker, and template) together in one polymerization phase and creating the pores. In the non-covalent approach, one needs to consider choosing solvents that promote template and functional monomer complex formation. In practice, special solvents, such as acetonitrile, methanol, and water in a particular ratio, can be used to create a strong template and monomer complex. For this thesis (**Papers I, IV and VI)**, I have studied MIP nanoparticles prepared using precipitation polymerization as described by Yoshimatsu *et al.*[52]

2.2.2 MIP nanoparticles with a core-shell structure

Due to the increasing demand of MIP nanoparticles in various applications, MIP nanoparticles with more complex structures have been developed. One synthetic approach is to use simple ***seeded emulsion polymerization***. Seeded emulsion polymerization is a two-step procedure that starts with the preparation of the core particles that serve as seed latex, using, for e.g., styrene,[53,54] DVB,[55] and methacrylate[56] as the monomers. The seed latex particles are generally monodisperse and can vary in size from approximately a few nm to several μm in diameter. In the second step, the seed particles are mixed with another monomer/mixture of monomers and polymerized, leading to the formation of MIP core-shell nanoparticles with binding cavities on the outer shell. Because of the presence of the uniform monodispersed core, the resulting particles have a controlled shape and size. Furthermore, the physical and chemical properties of the particles can be controlled by altering the composition and structure of the

monomers as well as the reaction conditions.[57,58] Peréz *et al.*[59] first synthesized MIP core-shell nanoparticles (76 nm in diameter) using an organic polymer seed latex as the core and produced a cholesterol-imprinted polymer shell. The core-shell emulsion polymerization proved to be effective in controlling both the size and the binding capacity of the nanoparticles. Peréz-Moral *et al.*[60] reported the non-covalent imprinting of propranolol in the shell of core-shell nanoparticles. The core-shell emulsion polymerization was carried out in the presence of the porogenic agent toluene, which led to increased surface area of the particles, resulting in high binding affinity in both aqueous and organic solvents.

For this thesis (**Papers II and III)**, I used MIP core-shell nanoparticles with a propranolol-imprinted core and amino-functionalized shell as reported by Hajizadeh *et al.*[61] The core particles were synthesized as previously reported by Yoshimatsu *et al.*[52] using precipitation polymerization (*cf.* section 2.2.1). To form a uniform hydrophilic shell, the core particles were mixed in the monomer solution consisting of allylamine, *N*-isopropylacrylamide (NIPA), and N,N'-methylene-bis-acrylamide (MBAAm) in the presence of the initiator AIBN and then polymerized. This one-pot, two-step precipitation polymerization yielded propranolol-imprinted nanoparticles with an amino-functionalized shell.

2.2.3 MIP microbeads by RAFT polymerization

Free radical (chain growth) polymerization is the most common method that is currently available for the preparation of MIP materials. The polymerization can be performed under mild reaction conditions (e.g., ambient temperature and atmospheric pressure) in bulk or in solution with a high tolerance to different functional groups (amino, carboxyl, hydroxyl, carbonyl, or ester). These reasons make this polymerization method most suitable for synthesis of MIPs. Radical polymerization can be initiated by heat, photoirradiation or redox reactions and is divided by three distinct stages: (1) initiation, (2) propagation, and (3) termination. Typically, in all free-radical polymerization, the rate of propagation (chain growth) is much faster than the rate of initiation, which results in the enormous growth of the polymer chain into a high molecular weight in a relatively short amount of time before the growth terminates. This process does not control the size and architecture of the resulting polymer.

To overcome these limitations and obtain a well-defined structure for the polymer material, "***controlled/living radical polymerization (CRP)*** " has emerged in the last decades. CRP comprises fast radical initiation combined with a slow but simultaneous chain propagation, resulting in a well-controlled final polymer product with a very narrow molecular weight distribution. The most common CRP chemistries used in molecular imprinting are atom transfer radical polymerization (ATRP), reversible addition fragmentation chain transfer (RAFT), and nitroxide-mediated polymerization (NMP).

RAFT polymerization is mediated by a chain transfer reagent (RAFT reagent), a thiocarbonylthio compound, which has compatibility with a large variety of monomers and does not require the use of a special catalyst.[62,63] Monomers capable of polymerizing by RAFT include styrene, acrylates, acrylamides, and many vinyl monomers. RAFT polymerization provides great versatility in providing polymers of predetermined molecular weight, low polydispersity, and different shapes and structures, such as comb-like structures, stars, brushes, linear structures, dendrimers, and cross-linked polymers. The resulting polymers may possess reactive end groups, which allow the attachment of the polymer to either another molecule or a solid substrate for different applications. Pan *et al.*[64] have reported different types of MIP spheres with good binding properties and water compatibility that were synthesized using RAFT polymerization. Titrici *et al.*[65] synthesized composite MIPs using a "grafting from" RAFT polymerization on silica particles. The MIP composites were synthesized using the "grafting from" method by CRP via RAFT. The mesoporous silica beads were modified with an azo initiator, and the graft copolymerization of MAA and EGDMA was controlled by the addition of the RAFT agent, a dithioester. The resulting composite MIP beads imprinted with L-phenylalanine anilide, as the template proved to be a highly efficient stationary phase in chromatographic separation.

In my research, MIP microbeads bearing thiol functional groups (MIP-SH) prepared by RAFT polymerization[66] were used. The nicotine-imprinted polymer microspheres were synthesized in two steps. In the first step, the polymer was prepared using MAA as the functional monomer, EGDMA as the cross-linker, AIBN as the initiator, nicotine as the template, and cumyl dithiobenzoate (CDB) as the RAFT agent. The RAFT polymerization resulted in MIP spheres with dithioester end groups. These end groups were then converted into terminal thiols by treatment with organic amines.[67]

2.3 Molecularly imprinted polymers in chemical sensors

The production of selective sensors requires a recognition element that is in close contact with a transducer surface. The recognition element should possess a specific chemical recognition element that allows a molecule, or a class of molecules, to be selectively recognized (bound) in a complex matrix. The transducer then converts the analyte binding signal into an easily quantifiable output signal. Many known biosensors have been reported where biological entities such as antibodies and enzymes were used as a recognition layer. There have been numerous attempts to replace the biological receptors with artificial ones to overcome the significant drawbacks of biological receptors, such as instability in changing physical and chemical conditions, expensive preparation, low yield, and the use of animals.

One answer to these shortcomings is molecularly imprinted polymers. MIPs are low-cost, fast to produce, reproducible, and sensitive compared to their biological competitors, making them suitable for various sensor applications. There are generally three approaches to report analyte binding by MIPs. The first is related to a special property of the analyte itself, e.g., MIPs synthesized in the presence of a nonfluorescent analyte analogue for the development of a fluorescent ligand displacement assay.[68,69] The second approach is the generation of an optical signal in a MIP catalysis reaction, which serves as an efficient transduction method for the analyte detection.[70] The third and most common approach is the interfacing of the polymer either *in situ*[71] or by immobilizing pre-made MIPs on the optically active transducer surface.[72] The resulting polymer surfaces can also be made optically active by surface conjugation with fluorescent molecules, quantum dots or metal nanoparticles.

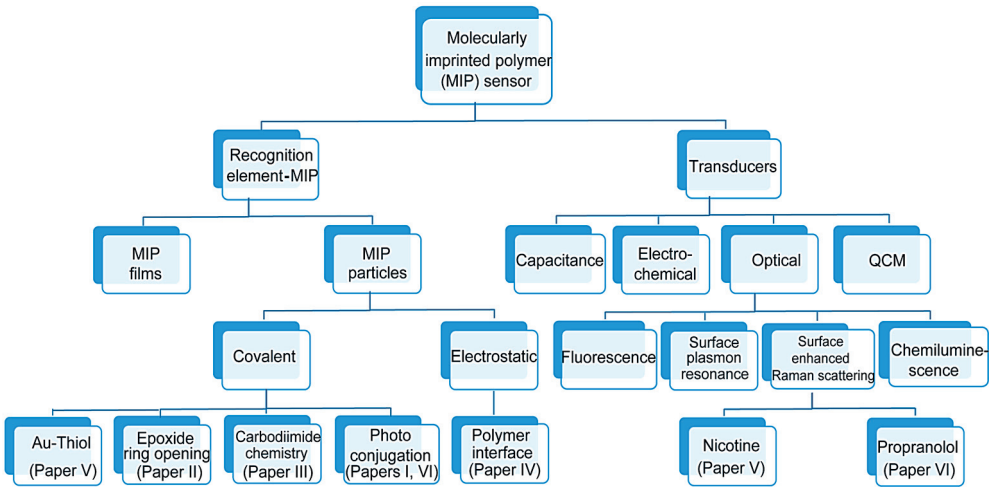

Figure 2.3. Schematic presentation of the MIP sensor study conducted in the thesis.

The MIP micro- or nanoparticles possess a large surface area and uniform spherical geometry, and their interfacing with the transducer surface provides increased chemical reactivity, binding capacity and kinetics, leading to many different chemical sensors.[73]

MIPs have been prepared for different sensing applications. Piletsky and Turner first developed a MIP sensor for domoic acid with a direct photografting of the polymer on the surface plasmon resonance (SPR) sensor surface.[74] Ye *et al.*[75] reported a MIP nanoparticle fluorescent sensor imprinted against a (S)-propranolol molecule by incorporating a scintillation reporter element (antenna molecule) in close proximity to the imprinted binding sites during the precipitation polymerization. The binding of the imprinted polymer with the ^{3}H labeled (S)-propranolol resulted in generation of the β radiation, which was effectively transferred via the antenna molecule to the scintillator, generating a fluorescent signal. Another MIP nanoparticle sensor was developed by Reimhult *et al.*[76] using quartz crystal microbalance (QCM) as the transducer surface for the propranolol detection. Figure 2.3 summarizes the different strategies described in this thesis for *ex situ* MIP nanoparticle immobilization and SERS-based MIP application. In the following sections 2.3.1 and 2.3.2, the integration of the MIP nanoparticles with the transducer supports and their optical template detection is described in detail.

2.3.1. MIP immobilization on a transducer surface

MIPs can be immobilized on the transducer surface either *in situ* as a polymer film[77-79] or *ex situ* as preformed nano- or micro-sized polymer spheres. This can be performed using different immobilization chemistries.[80] The *in situ* approach has been difficult to control, with a resulting large batch-to-batch variation. The thick MIP films grafted on the transducer also contain plenty of binding sites, but the underlying transducer has not been able to detect the signal beyond a certain distance (a few nm), e.g., in SPR and electrochemical measurements. These shortcomings led to the implementation of preformed MIP spheres with high template binding capacity on the transducer surface. Main strategies for immobilization of polymer spheres on a transducer rely on (1) physical adsorption, (2) entrapment in a polymer layer (gels, etc.), and (3) chemical grafting by means of covalent bonding.

As shown in Figure 2.4, there are different routes for the *ex situ* or preformed-MIP-nanosphere deposition on the transducer surface. Panel (A) shows how a few µl of MIP nanoparticle suspension in a suitable solvent is dropped on the functionalized transducer surface and left for solvent evaporation. This results in the MIP nanoparticles' attachment. Panel (B) shows incubation of the chemically modified transducer surface in the MIP nanoparticle suspension for a few hours, which allows the functional groups on the particles' surface to react with the underlying functionalized transducer surface (with and without an interlayer of linkers). The particles in the solution interact with the surface by means of attractive interactions. This interaction results in the stable and irreversible chemical bond formation between the MIP particles and the transducer. In panel (C), spin coating of the MIP nanoparticle suspension on the transducer surface is shown. To achieve a thin and uniform physisorption of MIP particles on the support, the particle size should be decreased because it is difficult to homogenously glue large particles onto the surface.[76]

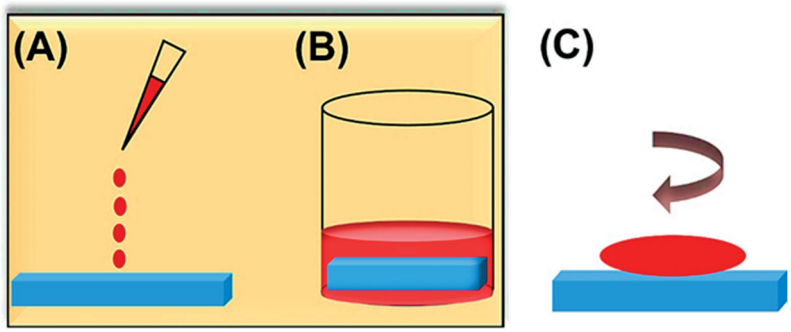

Figure 2.4 Different approaches for MIP-NP attachment on a transducer surface: (A) drop casting, (B) dipping in the MIP suspension, and (C) spin coating.

For this thesis, I used methods (A) and (B) for stable, uniform, and dense MIP nanoparticle immobilization on a solid transducer surface. The transducer surfaces functionalized with silanes, thiols, and photoactive molecules were either incubated in an MIP nanoparticle suspension or the suspension was drop casted on the patterned transducer surface for particle attachment. Microscopic and spectroscopic (*cf.* Chapter 3) investigation of the surfaces showed that both these approaches work well for a stable, dense and homogenous integration of the polymer spheres with the solid transducer surface for reliable analyte or template detection.

2.3.2 MIP nanoparticles for optical sensing

Most transduction methods are based on optical, resistive, surface acoustic wave (SAW) or capacitive measurements, as shown in Figure 2.3. Out of these methods, I used the optical methods, primarily due to their ease of operation, high sensitivity, and low cost. Optical techniques are invaluable due to their contribution to device miniaturization and lower limits of analyte detection.[81]

The basic principle behind the MIP-based optical sensor is described by the specific interaction of the recognition layer with the target analyte and its transformation into a detectable signal.[82] Compared to other optical sensor principles, such as SPR,[83,84] chemiluminescence,[85] and fluorescence detection methods (*cf.* Figure 2.3), Raman scattering has the advantage of producing very specific vibrational spectra that are characteristic of the template moiety bound to the molecularly imprinted polymer

surface. The technique is less affected by cross-selectivities due to non-specific adsorption, swelling, and shrinking of the polymer. This makes the technique easy, fast, and reliable. The detection of the Raman signal due to the inelastic scattering from the analyte is often very weak and difficult to detect. To overcome this problem, the concept of surface-enhanced Raman scattering (SERS) (described in detail in section 4.2) was introduced by Moskovits *et al.*[86] The first MIP-based SERS sensor was introduced by Kostrewa *et al.*[87] for the detection of (2S, 3S)-(+)-di-O-benzoyl-tartaric acid and N-benzyloxycarbonyl-(L)-aspartic acid.

One of the most important challenges in building MIP-based SERS sensors is to ensure that the MIPs carrying the molecular recognition sites are intimately integrated with the SERS-active surface so that the surface can effectively enhance the otherwise weak Raman signal. In previous studies, the MIP components were prepared *in situ* on Raman-active surfaces.[88,89] The *in situ* preparation is limited by the required quantity of noble metals, which is expensive and difficult to use on a large scale. To overcome these problems, I used an *ex situ* approach (*cf.* Section 2.3.1)

The *ex situ* prepared imprinted polymer spheres can be covalently integrated with different SERS transducer surfaces. These surfaces can be a roughened noble metal surface (e.g., silver or gold)[90-92] or a metal-coated rough porous surface[93-95] that can generate localized surface plasmons upon light irradiation. Kantarovich *et al.*[96] reported the use of a patterned SERS support, Klarite (registered trademark of Renishaw diagnostics, UK), to print MIP droplets and monitor the uptake and release of the *β*-blocker drug propranolol. Another paper reported the detection of explosive TNT using a MIP-based SERS sensor.[30]

MIPs can be combined with different optically sensitive materials, e.g., Au or Ag, to make them SERS active. One such approach was reported in 2010 by Bompart *et al.*,[29] which resulted in a SERS chemical sensor based on a MIP nanoparticle composite for the detection of propranolol. The sensing particles were core-shell particles with gold colloids located between the polymeric core and the very thin outer MIP shell, which made them SERS active. A different but similar approach using surface-imprinted core-shell Au nanoparticles was reported by Xue *et al.*[91] for the detection of bisphenol A (BPA) in environmental samples using the SERS approach. Another SERS-active metal, Ag, was used in the form of microspheres grafted with an MIP shell for the femtomolar detection of *N*,*N*-methylene-bis-acrylamide (MBA).[90] These core-shell MIP nanoparticles proved to be very

effective for the detection of analytes in real-life samples. The hot spots created by the metal colloids/nanoparticles help in even single-molecule detection.

In my studies, I designed SERS sensors for specific and selective detection of nicotine (**Paper V**) and propranolol (**Paper VI**) using preformed MIP spheres. In **Paper V**, the nicotine-imprinted MIP microspheres were synthesized *ex situ* using RAFT polymerization, leading to a high template (nicotine) binding property (see section 2.2.2). These spheres were then integrated with different transducer surfaces (an Au wafer and SERS-active Klarite) with Au nanoparticles and colloids attached on the particle's surface to produce the SERS nicotine signal.[97] Klarite surfaces feature a systematically designed array of inverted pyramids obtained using a lithographic-patterning of silicon surface followed by coating of a thin layer of gold.[98]

In **Paper VI**, I report on an MIP nanoparticle-based SERS sensor for propranolol drug molecule detection in human urine. The nanoparticles were synthesized *ex situ* using precipitation polymerization (see section 2.2.1) and immobilized on a SERS-active Klarite surface. The covalent attachment of the nanoparticles on the Raman-active surface was achieved using straightforward photoconjugation through a perfluorophenylazide linker, which proved to be simple, robust, and effective for sensitive propranolol detection. Thus, the SERS-based (optical) sensing of the template molecules can be implemented for the sensor construction with general applicability.

3. Experimental techniques

3.1 X-ray photoelectron spectroscopy

X-ray photoelectron spectroscopy (XPS) or Photoemission Spectroscopy (PES) is a surface-sensitive characterization technique based on the photoelectric effect, which was first discovered by Hertz in 1887[99] and later explained by Einstein in 1905.[100] Many years after the discovery, Siegbahn *et al.* developed this technique for the chemical analysis of surfaces. Siegbahn received the Nobel Prize in 1981 for his contribution to the development of the Electron spectroscopy for chemical analysis (ESCA) method, currently most often called XPS.[101]

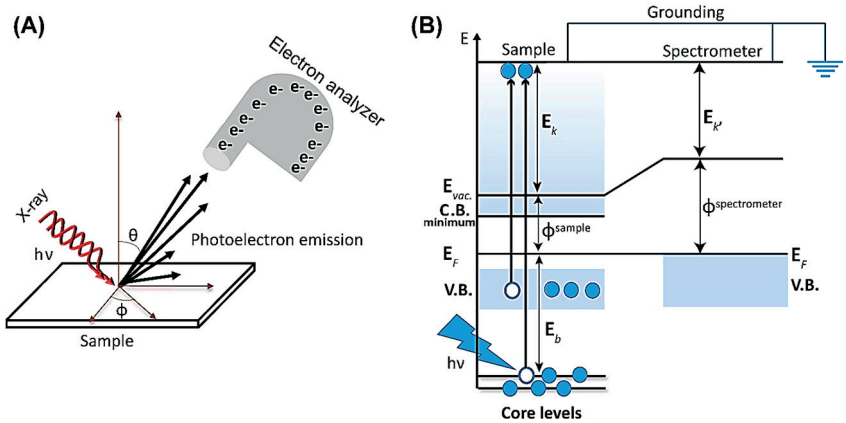

Figure 3.1. (A) Illustration of the photoelectric effect: X-rays with photon energy hν impinged on the sample surface, and electrons are emitted. The electron energy analyzer is oriented at an angle θ from the surface normal, referred to as the emission angle. (B) Schematic representation of the photoemission process, and the energy reference using a calibration to the Fermi energy (E_F) common to the sample and analyzer.

3.1.1 Theory

XPS is based on the photoelectric effect in which a sample is irradiated with X-ray beam with a well-defined energy hν. The irradiation results in the photoemission of electrons, which are collected by an electron energy analyzer as shown in Figure 3.1A. The photoelectrons are emitted from both the core and valence level of an element. The core-level energies are element-characteristic but, nevertheless, slightly differ in different chemical environments. Not only the number of photoemitted electrons but also their kinetic energy (E_k) are measured by the analyzer, which is kept at a grounding or reference potential (*cf.* Figure 3.1B). Equation (1) shows the relation of the measured kinetic energy $E_{k\prime}$ and the binding energy E_b of the electrons in the solid:

$$E_b = h\upsilon - \phi_{sample} - E_{k\prime}. \quad (1)$$

where ϕ_{sample} is the work function of the surface under study, i.e., the energy needed to remove an electron from the Fermi level of the solid to the vacuum level.

With respect to the analyzer, the kinetic energy of the emitted electron is represented as E_k' and is different from the E_k in front of the sample due to the differing vacuum levels of the sample and spectrometer. It is this E_k that is actually measured. Thus, according to the figure,

$$E_b = h\upsilon - \phi_{spectrometer} - E_k, = h\upsilon - \phi_{sample} - E_k. \quad (2)$$

As stated above, in X-ray photoelectron spectroscopy, photoemission from the core levels and the valence levels can be measured. In addition to the direct photoemission lines, one observes quantized satellites, a continuous background due to inelastic losses of the photoemitted electrons, and lastly the emission from Auger electrons.[102] Core levels, i.e., inner-shell levels, are highly localized to the photoemitting atom. They lead to the appearance of lines at binding energies characteristic of the photoemitting element. The interpretation of X-ray photoelectron spectra can be based on the so-called ***three-step model***[1], which divides the entire photoemission process into three steps.[103] Figure 3.2 shows the model: the first step is the photoionization, which is the photoexcitation of atoms located at various depths of the sample. In the second step, the photoelectron travels through the sample towards the surface, and in the third step, it finally escapes from the surface into the vacuum, where it is detected and its energy is analyzed.

The photoemitted electrons' energy is affected by many contributions, which together explain the spectral features and line profiles. One of the most important contributions results from the fact that the binding energy of a (core) electron is dependent on the charge density of the photoemitting atom. This results in the shift of the core-level peak in different chemical environments, referred to as the *chemical shift*. Chemical shifts, in this definition, are initial state effects.[104] The core-level spectra are also affected by other losses in the excitation of an atom and generation of a core-hole and further during the ejection of the photoelectron into the vacuum. These losses are termed intrinsic and extrinsic losses. During step 1 of the three-step model, i.e., in the creation of the final state, there are intrinsic losses due to the spin-orbit splitting (described below in detail), phonons (lattice vibrations), and shape-up and shake-off satellites. Phonon, shake-up, and shake-off losses, the latter two of which correspond to valence excitations to bonded (shake-

[1] Three-step model is somewhat superficial and the separation of stages is somewhat artificial. In theory, a correct description is obtained in the "one-step model" in which the whole process of photoexcitation, travel to and escape through the surface should be treated as one step.

up) or non-bonded (shake-off) states, decrease the kinetic energy of the photoelectron compared to the main line and thus appear at the higher binding energy side of this line.

Both quantized and non-quantized extrinsic losses can be incurred by the emitted electrons during their transport from the emitting atoms towards the surface (step 2) and their removal from the surface towards the vacuum (step 3) of the three-step model. The non-quantized inelastic scattering leads to a continuous background from the photoemission line down to zero kinetic energy. For metals, the creation of electron hole pairs at the Fermi level leads to an asymmetric broadening of the photoemission line. Quantized electron oscillations in the bulk (bulk plasmons) and at the surface (surface plasmons) show up as higher binding energy satellites, typically at some five to several tens of eV, to the photoemission line.

Another very important effect is the *Auger effect* behind Auger electron spectroscopy (AES). Also in XPS, Auger lines appear due to an autoionization decay of the core-excited atoms.[105] The photoemission process-produced core-excited state is an unstable state. The core hole is eventually filled by an outer shell electron. The energy gained in this decay is transferred to either another electron of the atom (Auger electron) or an X-ray photon (fluorescence). For low-Z elements with a core hole in the *K* shell, the Auger process is much more likely than fluorescence. Unlike the photoelectric lines, the Auger lines do not change kinetic energy when the incident photon energy is changed, which makes the Auger lines easy to identify. Thus, the Auger electrons have characteristic energies of the atom from which they arose and can be used for elemental identification.

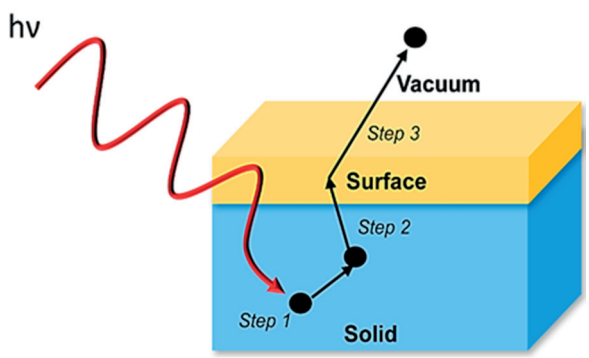

Figure 3.2. Schematic representation of the different steps involved in the three-step model, resulting in the photoemission process.[106]

To go into more detail, I will now consider the probability for a photoelectric transition. Here, σ is the transition probability per unit time for exciting a single atom or molecule from its initial state $\psi^i(N)$ to its final state $\psi^f(N)$. The electromagnetic wave is assumed as a time-dependent travelling wave of the form

$$A(r,t) = eA_0 exp[i(k_{h\nu} \cdot r - 2\pi\nu t)]. \quad (3)$$

where e is the unit vector in the direction of polarization, A_0 is an amplitude factor, and $k_{h\nu}$ is the wave vector of the propagation with ν as the incident wave frequency. The transition probability per unit time for the transition from $\psi^i(N)$ to $\psi^f(N)$ is proportional to the squared matrix element.[107,108]

$$|M_{if}|^2 = \left|< \psi^f(N) \left| \sum_{i=1}^{N} A(r_i).\beta_i \right| \psi^i(N) > \right|^2. \quad (4)$$

$$= \hbar^2 {A_0}^2 \left|< \psi^f(N) \left| \sum_{i=1}^{N} \exp[i(k_{h\nu}.r_i)]e.\nabla_i \right| \psi^i(N) > \right|^2. \quad (5)$$

Here, $\beta_i = -i\,\hbar\nabla_i$ is the vector potential of the field. Further, one can approximate that the photon wavelength λ is much larger than the photoexcited systems' dimensions (Å), which makes the element $\exp i(k_{h\nu}.r_i)$ unity. This is the so-called dipole approximation. In addition, for XPS, one can make the so-called "sudden approximation," which has proven to be very successful for predicting the intensities of various types of many electron fine structures observed in XPS spectra. In this approximation, the response of the system to the creation of the core hole is assumed to be instantaneous, and there is no interaction between the escaping photoelectron and the remaining final state system.

Under the dipole and sudden approximations, the transition probability, i.e., the cross-section, is proportional to

$$\left|< \phi^f|\hat{t}|\phi_k(1) >\right|^2 \left|< \psi^f(N-1)|\psi_R(N-1) >\right|^2 \quad (6)$$

and involves a one-electron matrix element and an (N-1) electron orbital overlap with $\phi_k(1)$ as the orbital from which the photoelectron will be emitted and $\psi_R(N-1)$ as the electron remainder state, the same way the final state consists of ϕ^f as the final state of the orbital from which the electron is emitted and its respective $\psi_R(N-1)$ remainder state.

To further simplify, one can make use of Koopmans' theorem.[109] Here, the relaxed state as explained by the "sudden approximation" is neglected, and one assumes that the orbitals other than that involved in the photoemission are the same in the final

and in the initial state. This is known as the frozen orbital approximation. In the initial state, the total N-electron energy, $E_i(N)$, is expressed as the one-electron energy of the k orbital, ε_k, and the remaining N-1-electron energy, $E_i(N-1)$, as

$$E_i(N) = \varepsilon_k + E_i(N-1). \quad (7)$$

If one assumes that the N-1 electrons in the ionic state do not feel the presence of the hole and remain in the same positions and energy as in the non-ionized state, then

$$E_f(N-1) = E_i(N-1). \quad (8)$$

By calculating the value of the initial and final energy states in a Hartree-Fock approach for non-interacting electrons, one obtains the final binding energy, $E_B(k)$ (the difference between $E_f(N-1)$ and $E_i(N)$), which is equal to the negation of the one-electron energy of that orbital from which the photoelectron is emitted, yielding

$$E_B(k) \simeq -\varepsilon_k. \quad (9)$$

This is the so-called *Koopmans' energy*. Koopmans' theorem applies only to closed-shell systems or to solids that contain many electrons in highly delocalized valence orbitals. This means that this theorem omits the fact that, after the ejection of a photoelectron from an orbital k, a positively charged core hole is generated. Electrons in the vicinity of the core hole will rearrange or screen the potential to reduce the energy. This final state effect resulting from electron readjustment is referred to as relaxation or the screening process. Therefore, the correct $E_B(k)$ is from that in Koopmans' approximation by a relaxation energy E_R:[103]

$$E_B(k) = -\varepsilon_k - E_R. \quad (10)$$

From the above approximations, it can be concluded that the binding energy of a photoemitted core electron depends on both the initial and final state of the system. In particular, the core-level binding energy is influenced by the chemical state or environment of the emitting atom. As stated above, this leads to a chemical shift. The shift is very useful to obtain information, e.g., about the surface functional groups, chemical environment, and oxidation state. An example of chemical shift is shown in Figure 3.3 (adapted from **Paper II**). An Si 2p spectrum of a clean silicon wafer (A) before any chemical functionalization shows intense bulk silicon peaks (Si $2p_{3/2}$ – 99.7 eV and Si $2p_{½}$ – 100.0 eV) and a broad surface oxide (SiO_2) peak at 103.5 eV binding energy, i.e., here a chemical shift is observed between the bulk

and surface oxide peaks. As is seen from spectrum (B), also after silane adsorption, an Si 2p line at approximately 103.5 eV binding energy is visible. This implies that the Si in the silane, which contains three methoxy groups bonded to the Si, has approximately the same Si 2p binding energy as SiO_2 and that it is difficult to distinguish between the silane and the oxide. In view of the very similar chemical environment of Si in both compounds, this is not particularly surprising, however.

Often, a special type of binding energy shift occurs between the bulk and surface atoms. It is referred to as the so-called *surface core level shift (SCLS)*[109,110] due to the difference in the chemical environment experienced by the core-level electrons in the solid and by the surface. The existence of such shifts is a considerable help in the study of adsorption on many surfaces, particularly metals.

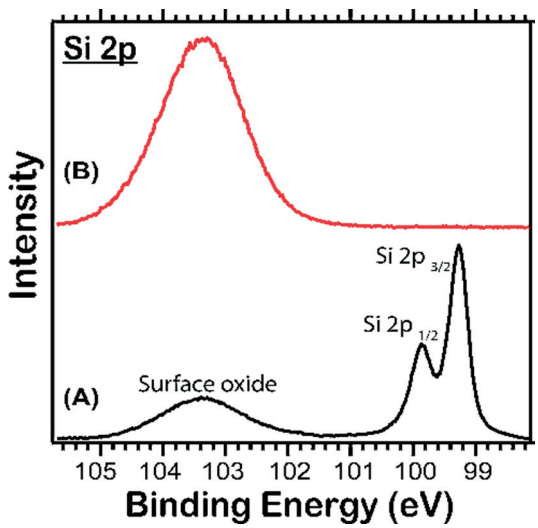

Figure 3.3. Si 2p spectra of (A) an oxidized n-type clean silicon wafer and (B) self-assembled monolayers (SAMs) of an epoxide functionalized silicon wafer representing the chemical shift. The degenerated peak at lower binding energy (Si $2p_{1/2}$ - 99.7 eV and Si $2p_{3/2}$ – 100.0 eV) is due to the bulk component, whereas the broad peak at higher binding energy, 103.5 eV, is due to the surface oxide component. Adapted from **Paper II**.

Electron mean free path

The surface sensitivity of the XPS primarily depends on inelastic scattering of the photoemitted electrons in the solid material and, to a much lesser extent, even elastic scattering. The inelastic mean free path (IMFP) is the key material parameter that describes the inelastic scattering. The IMFP is the average distance travelled by an electron with a specific energy in between its successive inelastic collisions. For solids, it is adequately described by[111]

$$\lambda = \frac{E_k}{E_P^2[\beta\, ln(\gamma E_k) - (C/E_k) + (D/{E_k}^2)]}. \quad (11)$$

Here, λ is the IMFP (in Å), E_k is the kinetic energy of the photoelectron (eV), E_P is the bulk plasmon energy (eV), and β, γ, C, and D, are material-dependent parameters. The equation shows the dependence of λ on the electron energy and the type of material.

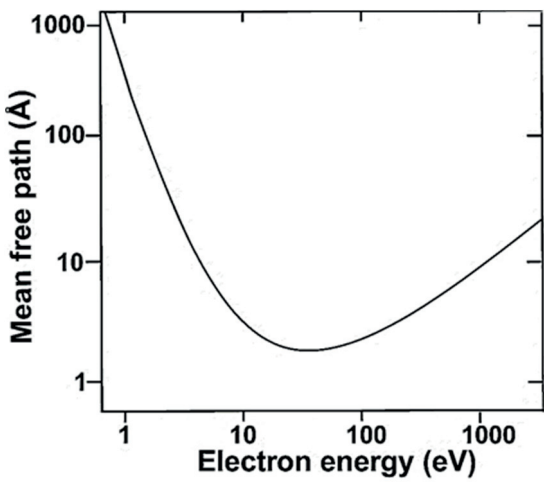

Figure 3.4. The "universal curve of surface science," representing the inelastic electron mean free path as a function of kinetic energy. The values for real materials are scattered around the curve but follow the general trend depicted here.[112] The universal dependence for a large number of elements is because the major interaction between the electrons in the solid can be approximated in terms of the electron density rather than the material-dependent bonding properties.

The IMFP (in Å) according to equation (11) as a function of electron kinetic energy (in eV) is shown in Figure 3.4. In principle, the mean free path is a characteristic property of a material, and thus the values for real materials are scattered around the plotted curve. All materials do follow the general trend, though. The minimum of the IMFP curve at approximately 50-100 eV kinetic energy corresponds to the maximum surface sensitivity. At this kinetic energy of approximately 5-10 Å, the surface layer are probed, which corresponds to the very top layers of the solid.

This implies that maintaining the energy range for the photoelectrons at approximately the minimum results in surface-enhanced measurements. Hence, the surface sensitivity of an XPS measurement can be tuned by controlling the photon energy (hν) of the incident radiation so that the kinetic energy of the photoelectrons is in the range of the minimum of the universal curve. In addition, another approach exists to render a measurement with surface sensitivity, namely by collecting the photoelectrons at a grazing emission angle, i.e., by performing *Angle resolved XPS (AR-XPS)*.

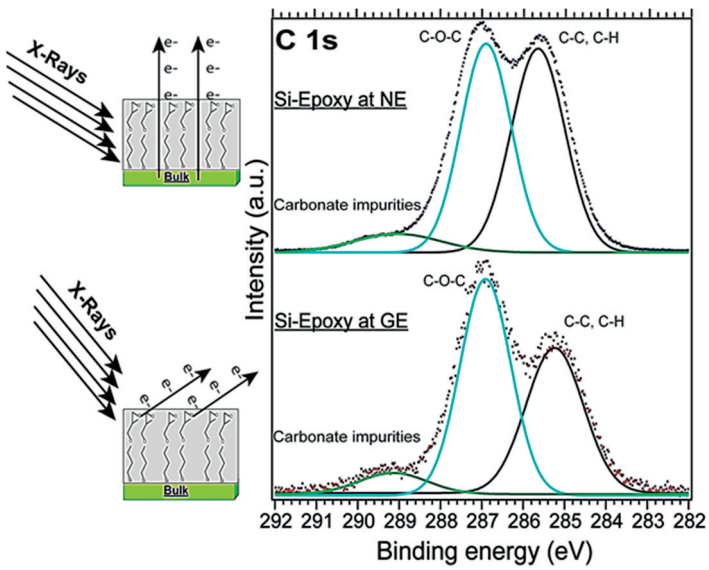

Figure 3.5. C 1s spectra of an epoxide-covered silicon wafer (Si-Epoxy) measured in normal (0° from the surface normal) and grazing emission (75°) geometries. The intensity ratio of the epoxide peak at 287.0 eV to that of aliphatic and adventitious carbon at 285.0 eV increases at grazing emission. Hence, the epoxy groups are located towards the surface of the epoxy layer. Figure adapted from **Paper II**.

In AR-XPS, the sample is tilted to different angles; thus, the angle of photoemitted electrons changes with respect to the surface normal, providing more or less surface sensitivity.[113] For Figure 3.5, the C 1s spectra of an epoxide-functionalized silicon wafer was recorded both in normal emission (0°) and grazing emission (75°) geometry. It is observed that, at normal emission, the main peak at 285.0 eV due to emission from aliphatic and adventitious carbon is almost of the same intensity as the peak at 287.0 eV related to the epoxide. At grazing emission, the intensity ratio of the aliphatic to epoxide peak decreases, which signifies that the epoxy groups are primarily located at the surface of the film, while the aliphatic and adventitious carbon is mostly located in the bulk.

3.1.2 Instrumentation

An XPS setup usually consists of a source of X-rays, vacuum system with at least high vacuum (10^{-8} to 10^{-6} mbar) or possibly ultrahigh vacuum (10^{-11} to 10^{-9} mbar), preparation chamber with a sample stage, stage manipulators and sample transfer devices, sample load lock, and electron detector system (hemispherical electron energy analyzer). Figure 3.1A shows the basic instrumental setup consisting of an X-ray source hitting the sample with a beam of photons of a particular energy hν. The emitted photoelectrons are collected by the hemispherical electron energy analyzer.

Traditionally used X-ray sources are gas discharge lamps, lasers, and monochromatic anodes. The most widely used are anodes producing Mg K_α radiation with 1253.6 eV of photon energy and Al K_α with 1486.6 eV of photon energy. The Fourier width half maximum (FWHM) of the non-monochromatic Mg K_α and Al K_α emission lines is roughly approximately 0.9 and 0.6 eV, respectively. Later, with a start in the 1940s and highly developed since the 1980s, electron accelerators were recognized as a very powerful light source of *synchrotron radiation* with a wide energy range providing “hard” X-rays (above 2 keV) or “soft” X-rays (below 2 keV).

Synchrotron radiation occurs when electrons with a velocity close to the speed of light are accelerated onto a curved trajectory, typically enforced by strong magnetic fields. The most commonly used electron accelerators for the production of synchrotron radiation today are electron storage rings, which use the bending

magnets, wigglers, and undulators for the acceleration of the electrons. Wigglers and undulators are cost-effective devices that generate highly intense photon beams in the straight sections of the electron storage rings. Figure 3.6A shows how a planar undulator works: an electron moving in a waveform through the up and down magnetic field produced by the periodically arranged magnets generates the synchrotron light. The wavelength range of the generated undulator radiation can be tuned to a particular value by variation of the magnetic field strength. The change in energy range is possible by tuning the periodic gap between the magnets (λ_U).

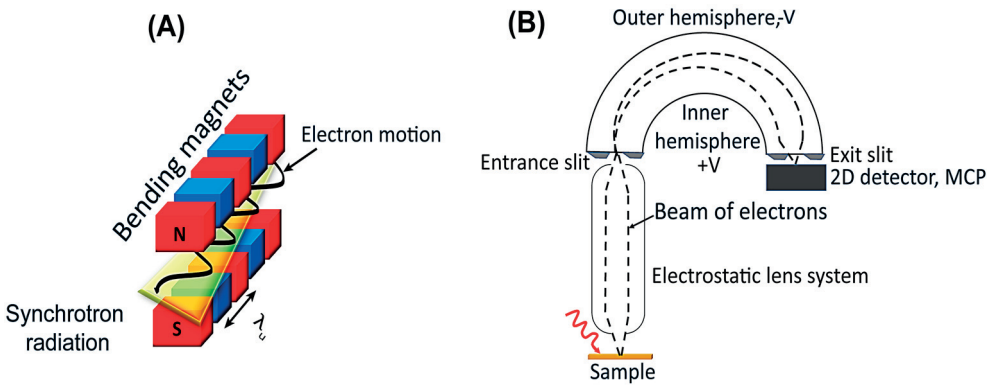

Figure 3.6. (A) Setup of an undulator consisting of a set of alternate bending magnets with a periodic length (λ_U) generating synchrotron radiation. (B) Schematic of a hemispherical energy analyzer.

Although the radiation from an undulator is in a narrow spectral region, the resolution is not sufficiently high for the experiment, and a monochromator on the beamline is used to monochromatize the radiation. For soft X-rays, reflection gratings are used. Finally, the focusing mirrors of different shapes focus the X-rays first onto the exit slit of the monochromator and then onto the sample in the experimental chamber.

The photoelectrons emitted from the sample in the analysis chamber towards the analyzer are focused by the electron optics system onto the entrance slit (*cf.* Figure 3.6B). The electrons then enter the space between the two concentric hemispheres, onto which different voltages are applied such that an electric field is created between the hemispheres, allowing electrons with a particular kinetic energy to pass

to the detector. This particular kinetic energy is referred to as the pass energy. Electrons emitted from the sample possess variable amounts of energy, and to allow the electrons with a specific kinetic energy to be detected, voltages are applied in the electrostatic lens system to retard or accelerate the electrons to the pass energy. Simultaneous detection of an entire energy spectrum (up to a certain width) and either the angular distribution or the location on the sample (in one direction) is possible using a two-dimensional detector. One such type, used in the present thesis, is a microchannel plate (MCP) stack combined with a phosphorescence screen and a charge-coupled device (CCD) camera. The measurements were carried out at the MAX IV Laboratory, Lund, Sweden at end stations I311[114] and I511[115] on the MAX II storage ring.

3.1.3 Data analysis

The energy resolution of the XP spectra is an important characteristic. The resolution has contributions from the instrumental broadening (X-ray source and spectrometer design) and intrinsic broadening. In addition, as mentioned above, the spectra include a background that is due to the inelastic scattering of the photoelectrons (*cf.* Sec 3.1.1).

In principle, spectral features have a Voigt lineshape, which is a convolution of Gaussian and Lorentzian distributions.[116] The Lorentzian contribution is due to the lifetime of the (core-) excited state with a width that essentially is the inverse of the lifetime. The Gaussian contributions primarily come from the instrumental broadening. However, for solids, the phonon broadening (excitation of the lattice vibrations) is typically not resolved, and the same can be true for the superposition of lines due to chemical shifts. Therefore, core-level spectra obtained on solids normally do not allow the direct measurement of excited state lifetime and instrumental broadening, although there exist exceptions. Although Voigt lineshapes often are used in the curve fitting of spectra measured in solids, their parameters are typically phenomenological rather than physical.

To perform a quantitative analysis, I removed the background from the spectra and fitted the components. The background is always adjusted to the high or low binding energy parts of the spectrum. There are three types of background that are most commonly used: linear, Shirley, and polynomial. I have mostly used Shirley and

polynomial backgrounds. The Shirley is a background subtraction technique[117] that iteratively adjusts the background as a function of the intensity of the photoelectric line.

A quantitative analysis must take *spin-orbit splitting* into account, which occurs due to the electromagnetic interaction between the electrons spins(s) and their orbital angular momentum (l) generated by the electrons' motion around the nucleus. It occurs for unfilled shells. In the present case, only the spin-orbit splitting due to the core hole created in the photoemission process is of relevance. Spin-orbit splitting in the valence states does not play any role here. The phenomenon of spin-orbit splitting is observed for emission from electron orbitals with $l > 0$. After the ejection of the photoelectron, an atom is left with a core hole. With this core hole, both s=1/2 and l are associated, and they couple into two states with different j quantum numbers. Because these two states have different energies, the energy of the outgoing electron is also affected, giving rise to a more or less closely spaced doublet with two different binding energies. The peaks will also have specific area ratios based on the degeneracy of each j state. For example, in Figure 3.3(A), one can observe an Si 2p spectrum with the bulk silicon peak split into the j= 1/2 and 3/2 components because the 2p core hole has l=1 and s = ½. The split peak with higher j value (3/2) has the lowest B.E. state or higher K.E. (due to favorable alignment of the core-hole spin and orbital angular momentum). The opposite happens for the component with lower j value (1/2).

3.1.3.1 Data calibration

Calibrations of the XP spectra are required for the following reasons. First, reliable comparison of the XPS data from two or more XPS instruments requires data calibration. Second, the same is true for a reliable identification of the chemical state. In my thesis, I used inorganic surfaces, silicon and Au wafers, for particle immobilization. The obtained XP spectra were calibrated according to a line of the underlying element, i.e., Si and Au.

All spectra in **Papers I, II, and IV** were calibrated by reference to the Si 2p peak for silicon dioxide at 103.5 eV binding energy.[118] In XP spectra of a clean Si wafer, Si 2p lines of both bulk Si and the surface silicon oxide (SiO_2) layer were observed. The Si 2p line exhibits a spin-orbit split doublet with the Si $2p_{½}$ component at 99.3 eV and the Si $2p_{3/2}$ component at 99.8 eV. However, in the oxide Si 2p line at 103.5 eV, the spin-orbit splitting is not resolved. The Si 2p line was recorded for each surface in question at the same setting as the other core-level lines, which enabled their calibration. The amount and the type of dopant (n- or p-type) concentration also affects the appearance of SCLS in the bulk silicon peaks.[119] This shift is due to the dopants' concentration gradient in both bulk and the surface, which affects the Si 2p core level spectra. However, the SCLS is not considered here for the calibration.

For the MIPs immobilized on the Au wafer (**Paper III**), the spectra were calibrated to the Au $4f_{7/2}$ peak of the sample at a binding energy of 84.0 eV, which is the Au $4f_{7/2}$ binding energy of bulk Au with respect to the Fermi level. Additionally, the Au 4f is spin-orbit split: the Au $4f_{7/2}$ component is at 84.0 eV and Au $4f_{5/2}$ at 87.5 eV binding energy, calibrated to the Au Fermi level. The calibrated Au 4f line was then used for calibration of the lines of the other elements. However, the Au $4f_{7/2}$ core-level peak also shows a broad shoulder at a lower binding energy (SCLS) due to the presence of surface features (*cf.* sec 3.1.1).[120] The SCLS and surface-to-bulk intensity ratios yield structural information.

3.2 Raman spectroscopy

The Raman effect was introduced by Sir C.V. Raman in 1928.[121] The spectroscopy technique based on the effect, Raman spectroscopy, is a fast and non-destructive method for optically probing the characteristic molecular vibrations, or "fingerprints," of an unidentified molecule through inelastic scattering. This spectroscopy is different from standard IR spectroscopy in that it is based on scattering rather than absorption. No tedious sample preparation steps are required, and the obtained vibrational information regarding the chemical bonds and structures is very specific.

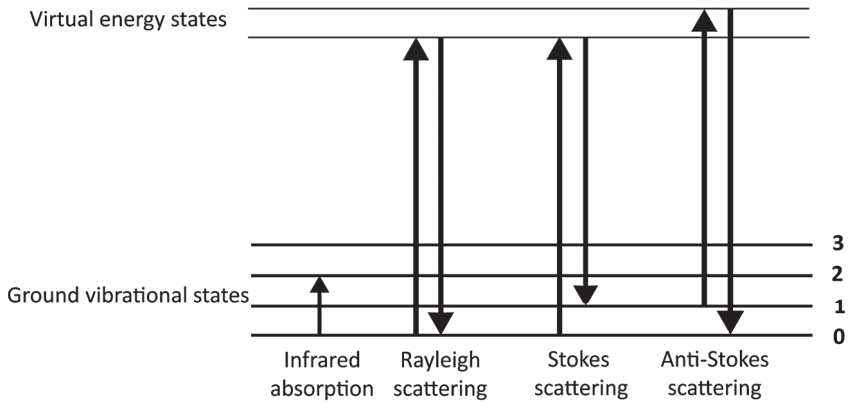

Figure 3.7. Jablonski energy diagram showing scattering processes involved in Raman spectroscopy.

3.2.1 Theory

When monochromatic radiation is incident upon a sample, the light interacts with the sample and can either be reflected, absorbed, or scattered. Figure 3.7 shows a Jablonski energy diagram representing the scattering processes involved in Raman spectroscopy. The photon interaction excites the molecule originally in a vibrational-rotational state of the electronic ground state to an excited vibronic state or a 'virtual energy state' (short-lived excited or intermediate state) before the deexcitation to the final state, which is the same electronic state as the initial state but the vibrational or rotational state might be different. A complete Raman spectrum consists of a peak due to Rayleigh scattering (same wavelength as excitation), a series of stoke-shifted peaks (longer wavelength as excitation), and anti-stoke peaks (shorter wavelength). The difference in energy is compensated for by the change in the rotational and vibrational energy of the molecule. Raman shifts are normally reported in wavenumbers υ (the inverse of wavelength) in cm^{-1}. The Raman shift is

$$\upsilon = \left(\frac{1}{\lambda_{\mathrm{Exc.}}} - \frac{1}{\lambda_{\mathrm{Scat.}}}\right). \qquad (12)$$

Here, $\lambda_{Exc.}$ is the excitation wavelength, and $\lambda_{Scat.}$ is the wavelength of the scattered light. According to the classical description of inelastic Raman scattering, a molecule, when put into an electric field, will be distorted with an induced dipole moment (μ). Consider an electromagnetic wave with an electric field vector $\vec{E}$ with an oscillating frequency ν and electric field amplitude($\vec{E}_0$):

$$E = E_0 \cos(2\pi\nu_0 t). \quad (13)$$

The induced dipole moment depends on both the electromagnetic wave and the polarizability α of the molecule, which is a tensor due to its anisotropic nature:

$$\mu = \alpha(\nu) \cdot E_0 \cos(2\pi\nu_0 t). \quad (14)$$

If a molecule is subjected to a laser light with the time-varying electric field, then the polarizability of the molecule also becomes a time-dependent quantity that depends on the vibrational frequency of the molecule ν. Thus, $\alpha(\nu)$ can be expressed as

$$\alpha(\nu) = \alpha_0 + \left(\frac{\delta\alpha}{\delta Q}\right)_0 Q. \quad (15)$$

where Q defines the vibration of the molecule, expressed as

$$Q = Q_0 \cos(2\pi\nu_m t). \quad (16)$$

Here, $\left(\frac{\delta\alpha}{\delta Q}\right)_0$ defines the rate of change of polarizability with the displacement at the equilibrium position of the molecule. The quantity Q_0 is the vibration of the molecule at its equilibrium position, and ν_m is the frequency of the vibration. Substituting equation (16) in equation (15) and then placing equation (15) into equation (13) results in

$$\mu = \alpha_0 \vec{E}_0 \cos(2\pi\nu_0 t) + \frac{1}{2}\left(\frac{d\alpha}{dQ}\right) Q_0 \vec{E}_0 \left[\cos 2\pi\left((\nu_0 + \nu_m) - (\nu_0 - \nu_m)\right)t\right]. \quad (17)$$

Equation (17) shows the dependence of the induced molecular polarizability on three different frequency elements. The first element has a frequency that is the same as the incident radiation frequency ν_0, referred to as Rayleigh or elastic scattering. The second and third terms have a frequency different from that of the incident radiation and are referred to as Raman or inelastic scattering. The Raman component at higher frequency ($\nu_0 + \nu_m$) is denoted as anti-stokes scattering and that at lower frequency ($\nu_0 - \nu_m$) as stokes scattering (*cf.* Figure 3.7).

3.2.2 Instrumentation

Raman spectroscopy requires monochromatic laser light as the excitation source. This intense source enables the measurement of small Raman shifts with good spatial resolution and a relatively good signal-to-noise ratio. The light source of a Raman spectrometer can range from the ultraviolet wavelength regime to the visible and near-infrared depending on the application. In my setup, the laser light was in the near-infrared regime with a wavelength of 785 nm. Lower photon energies are suitable to prevent electronic transitions resulting in fluorescence, thus making the Raman signal easily detectable. The only disadvantage with the higher wavelength is the decreased scattered light intensity, which is compensated for by increasing the integration times.

Figure 3.8 schematically shows the Raman setup used for the measurements. The light beam enters the Raman probe via fiber optics. It is then focused onto the solid sample using a collimator. The collimator helps to maintain a particular distance between the probe and the sample. The scattered light then passes a filter that only allows inelastically (Raman) scattered light to enter the detector. The photocurrent from each wavelength is measured at a charge-coupled device (CCD) detector, the output of which is transferred to the computer (data recorder) and viewed using a particular piece of software.

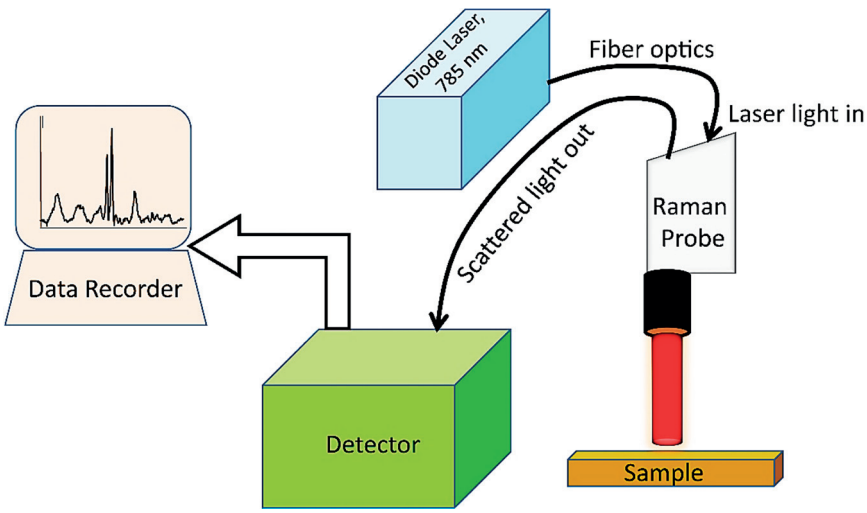

Figure.3.8. Instrumental setup for Raman measurements used in this thesis.

3.2.3 Surface-enhanced Raman spectroscopy

Normally, the Raman signal intensity is much weaker than that of elastic or Rayleigh scattering. In the case of solids, the signal intensity is 10^6 times weaker than that of elastic scattering. This problem can be overcome using the surface-enhanced Raman scattering (SERS) technique, a technique suitable for detecting even small quantities of analyte, down to picomolar concentrations. This technique enhances the Raman signal of molecules by their attachment on rough metal surfaces or colloids. It was reported for the first time by Martin Fleischmann, Patrick J. Hendra, and A. James McQuillan when they studied a monolayer of adsorbed pyridine molecules on a roughened silver electrode.[122]

3.2.3.1 Theory

SERS arises from two mechanisms, an ***electromagnetic*** and a ***chemically enhanced*** one.[123] The first and the most important is the enhancement of the electromagnetic field by the surface of nanostructured metal. Interaction of the light field with a smooth metal surface can result into six-fold enhancement in contrast, while a roughened metal surface can provide an up to 10^{11}-fold enhanced Raman signal of the adsorbed molecule's Raman intensity. The basic mechanism involved in electromagnetic enhancement is illustrated in Figure 3.9. Here, I considered a roughened surface consisting of metal spheres or nanoparticles. When the wavelength of the incident light is in resonance with the plasma wavelength of the metal, conduction electrons in the two metal spheres are excited to a collective higher-energy state, resulting in so-called localized surface plasmons. The metal spheres or chemically etched metal roughness features become polarized, which separates the conduction electrons from their opposite charge in the direction opposite to the incident electric field. The plasma oscillation enhances the intensity of the incident electromagnetic radiation used for exciting the Raman vibration modes of the molecules adsorbed on the surface. Thus, the Raman scattering signal is enhanced by a factor as large as 10^{10} to 10^{11}.

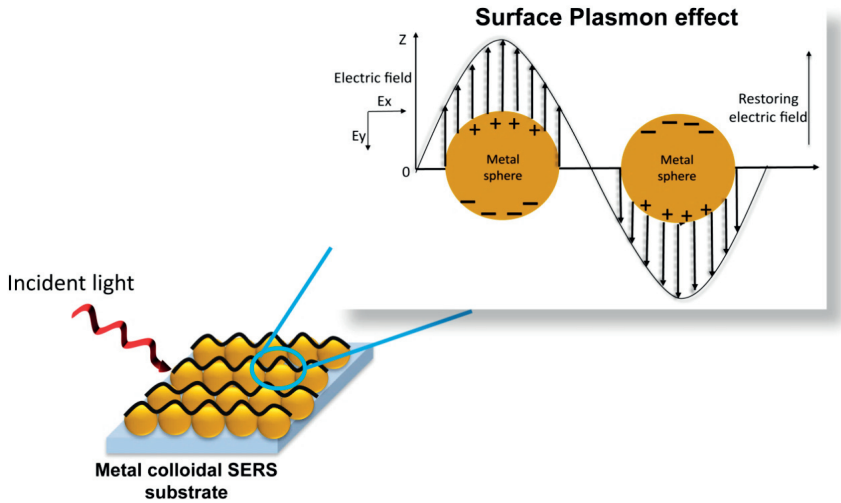

Figure.3.9. Illustration of the principle behind surface plasmon oscillations and electromagnetic signal enhancement in SERS.

The intensity of the Raman scattered radiation (I_R) is proportional to the square of the magnitude of the incident electromagnetic field on the target or detection molecule (E),

$$I_R \propto E^2. \tag{18}$$

E depends on two components:

$$E = E_a + E_p. \tag{19}$$

Here, E_a is the electromagnetic field of the target molecule in the absence of surface roughness, and E_p is the electromagnetic field emitted from the molecule on a roughened metal surface.[124] E_a is relatively small due to the flat nature of the metal surface that generates the plasmons but does not radiate them for the electromagnetic field enhancement, whereas E_p results in a large signal enhancement as the molecule adsorbed on the metal creates an additional radiating electromagnetic field due to the plasmons in close proximity to the molecule.

The second mode of signal enhancement is the charge transfer between the adsorbed molecule and metal surface. This mechanism provides an order or two of magnitude enhancement in the Raman signal.[125] Many molecules have a lone pair of electrons or π clouds, and they interact with the surface atoms. When the incident light energy

is in resonance with or higher than the electronic transition energy, then the charge transfer takes place from the adsorbate to the metal. This results in the change of the polarizability of the adsorbate molecules, resulting in the induced dipole or the enhancement in the Raman signal. It is interesting to note here that the molecular orbitals of the adsorbate broaden into the conduction electrons of the metal surface underneath, resulting in an alteration of the nature of the adsorbate. Many aromatic groups, such as phenols and pyridine, oxygen, and nitrogen-containing molecules are extremely SERS active.

A well-defined example showing the SERS phenomena using the chemical interaction was explained by Jiang et al. in 1987.[126] In this experiment, the pyridine molecules were chemisorbed at local defect sites on a smooth Ag adatoms surface, which resulted in a very small degree of enhancement, a factor of approximately 15- to 65-fold. There are many factors that affect the signal enhancement, such as the wavelength of the incident electromagnetic radiation and the morphology of the surface. It is observed that single spheres do not possess very high signal enhancement, irrespective of the wavelength. The reason for this is the absence of highly localized plasmon regions, which can only be observed in the junctions between two particles ("hot spots").[127] For example, for a 10-nm dimer, the enhancement occurs when the wavelength is in the near-infrared region. It can also be seen that a small decrease in interparticle distance (from 5.5 nm to 1 nm) yields an enhancement in the signal. For larger spheres or ellipsoidal-shaped particles, signal enhancement is possible at longer wavelengths.

3.2.3.2 SERS substrates

Several types of SERS substrate morphologies have been reported.[128] The most commonly used substrates for analytical applications are either metal colloidal suspensions or electrochemically roughened substrates (metal electrodes or inorganic surfaces coated with metals). The metals for SERS enhancement can be integrated with target molecules (polymer colloids in **Paper V**) using different interactions: physisorption, covalent, or electrostatic. The enhancing metals used are Ag, Au, Cu, Pt, and Na, but the most widely used are Ag and Au, as their plasmon frequencies fall in the visible and near-infrared wavelength region.

The most common and easiest approach reported is to use an Ag or Au colloidal solution. Moskovitis et al. reported the SERS spectra of pyridine molecules adsorbed on Ag islands (5-20 nm) and colloidal Ag assemblies (20 nm).[129] The SERS spectra showed a maximum signal enhancement on the order of 10^6. The metal colloids can be synthesized by a traditional method and integrated with the target (solid surface, polymer colloids, and molecules) by dipping the target into the colloidal solution.[130] The amount of colloids or nanoparticles can be tailored by controlling the concentration of colloids in the solution. The metal colloids or nanoparticles interact with the polymer colloids using either electrostatic or covalent attachment (**Paper V**). Recent developments in nanoscience fabrication have made it possible to structure metal templates for target material attachment. Various nano- and microstructured materials have made it possible to enhance the signal detection.[131] The most widely used SERS substrates for analyte detection are either Au or Ag colloid (20 nm)-patterned alumina surfaces, as reported by Zhang *et al*.,[132] or the lithographically patterned Klarite surface (Figure 3.10) reported in **Papers V and VI**.

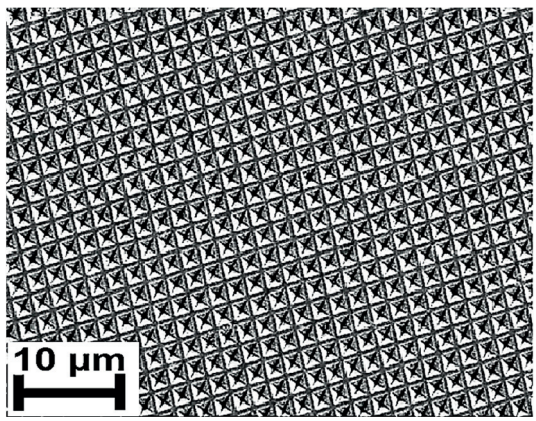

Figure.3.10. Lithographically patterned Au substrate (Klarite).

3.3 **Atomic force microscopy**

Atomic force microscopy (AFM) can achieve images of surfaces with atomic resolution. Developed by Binning, Quate, and Gerber, the technique is the successor to the invention of scanning tunneling microscopy (STM) in 1986.[133] In contrast to STM, AFM does not depend on a current between the tip and the sample, thus it is suitable even for non-conducting samples.

3.3.1 Theory

Atomic force microscopes consist of a probe or cantilever that maintains close contact with the sample and scans the surface. The force between the tip and the sample can be either attractive or repulsive. In response to the force between the tip and the sample, the cantilever tip is deflected. The piezocrystal attached to the cantilever helps in maintaining the lateral position in the x, y, and z directions for accurate measurement of the surface topography.

Figure 3.11 shows two different modes of AFM operation. First is the ***contact or static mode***. In this mode, the tip is in complete contact with the surface and is dragged across the surface. When the atoms of the tip initially come into contact with the atoms of the sample, they experience a repulsive force due to the overlap of the electronic orbitals of the tip and the sample at atomic distances. This results in the deflection of the tip, which eventually results in deflection of the laser beam. This change in the optical signal can be measured by the photodetector. The only problem in this mode is that the tip can exert significant pressure on the sample surface, thus resulting in damage to it. This is remedied in the second mode, which is termed the ***dynamic or non-contact mode***. In this, the cantilever is vibrated at a constant oscillating amplitude or frequency. As the tip approaches close enough to the sample, the attractive force (van der Waals, electrostatic, capillary forces) between the tip and sample causes changes in both the amplitude and phase of the cantilever vibration. These changes are monitored by the feedback loop to control the tip-sample distance. Sometimes while analyzing the samples in ambient atmosphere, it is critical to maintain the tip-sample distance at a certain constant

value and prevent the tip from coming into complete contact with the sample's surface. This brings us to the intermediate mode, the ***tapping mode***. In section 3.3.2, I discuss the tapping mode in detail.

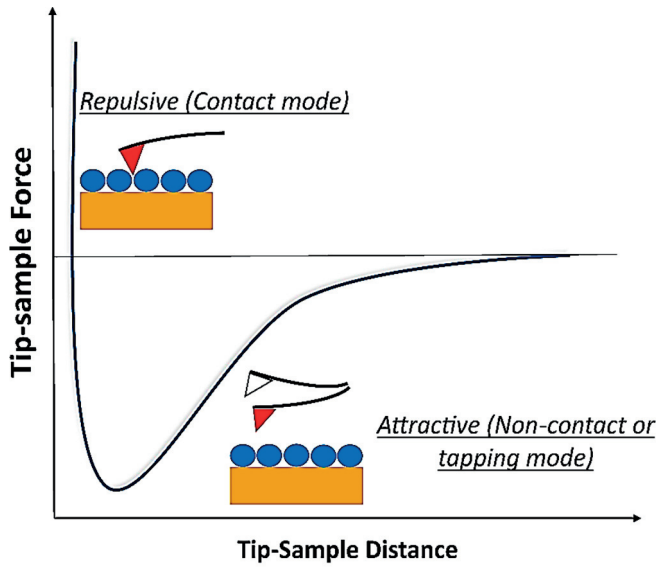

Figure.3.11. Force-distance curve representing the two modes of AFM, contact and non-contact.

3.3.2 Instrumentation

Figure 3.12 schematically shows the basic components involved in AFM. It consists of three important parts: the optical head, which detects the laser deflection; the piezoscanner head for controlling the scanning motion of the cantilever in the x, y, and z directions; and the detection electronics, which convert the measured optical signal into an image.[134]

AFM includes a tip mounted on a micromachined cantilever acting like a spring with a spring constant of 10-130 N/m. To obtain atomic resolution, the tip should be as sharp as possible; for my measurements, I used n-doped silicon cantilever tips with a typical curvature radius of 10 nm. The force on the tip due to the interaction with the sample results in the deflection of the cantilever being sensed as an optical (laser) beam deflection. The optical beam proved to be accurate and sensitive

enough to distance changes. The piezocrystal maintains the xyz motion of the cantilever to a constant height. AFM scans the sample in a raster fashion.

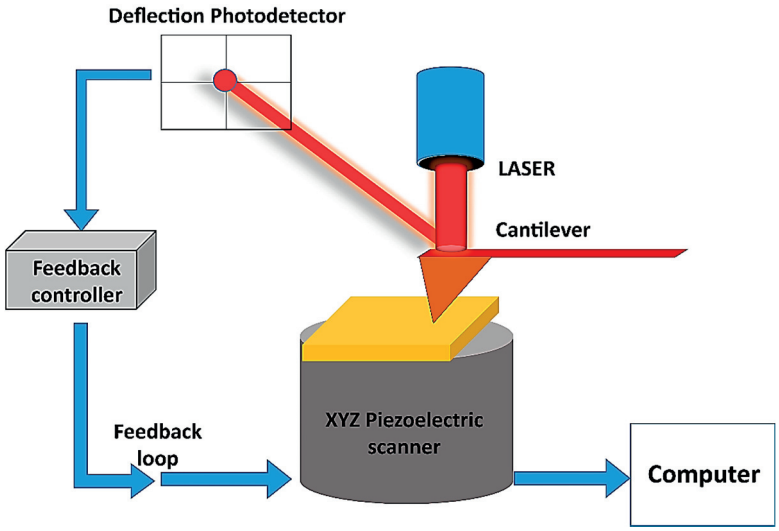

Figure.3.12. AFM instrumentation.

The AFM instrument used in this thesis was a Veeco Digital Instruments multimode scanning probe microscope, which uses an intermittent contact tapping mode. While scanning the surface, the cantilever tip undergoes vertical sinusoidal vibration with a resonant frequency of 204-497 kHz. The constant force feedback mechanism helps to scan the rough features on the surface without crashing the cantilever tip. The tapping mode minimizes the friction or other forces that could damage the surface, thus making this mode useful for even soft surfaces. In my system, the topographic measurements were performed on spherical, large-sized, soft polymer spheres immobilized on glass and silicon wafers (images shown in **Papers I-IV**).

3.4 Scanning electron microscope

For imaging of nanometer-sized objects, optical microscopy is not a suitable technique as the objects are much small than the wavelength of the light, which makes them impossible to identify under the normal microscope. Thus one has to

use a higher resolution technique instead, e.g., a high-resolution scanning electron microscopy (SEM). The SEM instrument was first invented by Manfred von Ardenne in 1937[135] but presented later by McMullan in 1995.[136] The first microscopic images of the solid samples were already published by Knoll and his group in 1935.[137,138] SEM is a technique which uses electrons to scan the sample and produce the image. The beam of electrons interacts with sample's surface atoms to give topographic information of the surface. The data is collected by scanning a selected sample area ranging from a few cm to microns to nm. Sample resolution at less than 10 nm can be achieved.

3.4.1 Theory

In SEM, an electron beam with a sufficient kinetic energy is incident on the sample and generates secondary electrons, backscattered electrons, and in some cases visible light and heat. The secondary (inelastic) electrons are detected using a secondary electron detector or scintillator. Depending on the number of electrons emitted the detector modulates the brightness level on the monitor. Other emissions such as the backscattered (elastic) or the X-ray photon emissions are detected using different sensors and result in an intense material contrast. Figure 3.13A shows the different emissions resulting from the electron interaction with the sample. The characteristic X-rays are generated due to the photoelectron emission from the sample and can be recorded using a spectrometer for energy dispersive x-ray spectroscopy (EDX) attached to the SEM.

3.4.2 Instrumentation

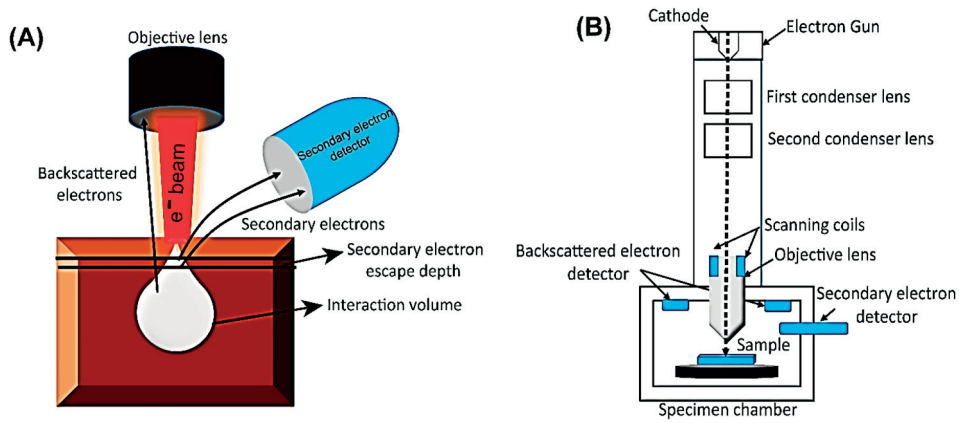

Figure 3.13. (A) Different signal types generated after the interaction of the electron beam with the sample. (B) Schematic setup of a scanning electron microscope.[139]

Figure 3.13B shows that the SEM consists of an electron gun, condenser lenses, sample chamber, and a detector. The electron gun emits the beam of free electrons either generated thermionically by a tungsten filament cathode or through field emission. Thermionic electron emission occurs when the tungsten filament is heated to a high temperature and the produced electrons leave the filament tip and are accelerated through the grounded anode with a high potential towards the microscope. In the field-emission gun, a sharp metal tip (typically radius of less than 100 nm) is used and a potential is applied between the anode and the tip resulting in an electron emission. Field-emission guns give much more brightness than the thermionic system because of the monochromatic electron source and a sharp tip.

After the beam passes the anode it is focused by a condenser lens system to form a ‘probe’. The electromagnetic lens system focuses the probe beam resulting in its small diameter and better resolution. After focusing the beam passes through one or more apertures consisting of a pair of scanning coils. The purpose of these apertures is to reduce and exclude the unfocussed electrons. The final lens aperture then determines the diameter or spot size of the beam directed towards the specimen.

Decreasing the spot size will result in the increase of the resolution. Other factors affecting the resolution of the image are corrected by the stigmators.

SEM of immobilized polymer spheres on solid surfaces is difficult under the electron microscope due to charging. To avoid this problem, the surfaces were coated with a few nm (10- 40 nm) of platinum (Pt) metal before inserting them into the SEM chamber. After mounting the metal coated samples on the sample holder, they were grounded using conducting carbon tape. The images were recorded in secondary emission mode with a shortest possible distance from the electron gun. The gun voltage of 10 kV and a vacuum pressure of 5×10^{-6} mbar were used to obtain bright high resolution images.

4. Results and Discussions

This chapter is divided into two parts. The first part addresses the **different immobilization chemistries** used to achieve a stable, homogenous, and dense MIP nanoparticle coverage on different solid supports (section 4.1), and the second part addresses an **application-based study of the use of MIP micro- and nanospheres** on gold-coated transducers for the detection of nicotine and propranolol (section 4.2).

4.1. Immobilization chemistry

Physisorption can be used in a well-known, easy, and fast approach for the attachment of MIP nanoparticles or spheres on a solid surface. However, physisorption is problematic, because adsorbed particles may be released from the surface that they are attached to when the surface in the sensing process is immersed in the analyte solution due to the weak interaction strength of the particles with the surface. Additionally, physisorption results in an inhomogeneous MIP distribution, which can lead to an unreliable signal from the MIP-modified surface. These problems can be overcome by using chemical grafting approaches. First, chemical grafting binds the polymer spheres strongly to the surface and avoids their release into the solution during analyte binding and washing; second, it reduces the background noise due to non-specific adsorption. This makes chemically grafted MIP nanoparticle surfaces reusable after regeneration. There are different immobilization or chemical grafting approaches, but one has to choose the most suitable strategy depending on the molecules to be immobilized on a specific transducer support. Indeed, the transducer is not chosen for its ability to be grafted but for its capability to transduce the chemical signal generated after the binding event.

In this dissertation, I report the use of inorganic materials' surfaces, such as silica, glass, and gold. There are few selected approaches compatible with immobilizing MIP nanoparticles on these surfaces. I report the use of hetero-bifunctional molecules with their one end attached on the surface and the other exposed for immobilizing MIP nanoparticles covalently (**Paper I-III**) or electrostatically (**Paper IV**).

4.1.1. Covalent immobilization

In the work for this thesis, I have used nano- and micro-sized polymer particles imprinted against propranolol and nicotine with and without a functional shell structure. The polymer spheres can be used for label-free sensing applications if they are immobilized covalently on the transducer (*cf.* section 2.3, Chapter 2).

4.1.1.1. Photoconjugation chemistry

In **Paper I**, a methodology for immobilization of propranolol-imprinted MIP nanoparticles on a glass substrate was studied. Figure 4.1 shows the steps involved: in the first step, the glass surface was functionalized with 3-aminopropyltriethoxy silane (APTES) which generated amino groups that act as binding groups for the stable, dense, and homogenous attachment of perfluorophenylazide (PFPA). In the second step, the amino groups were reacted with *N*-hydroxysuccinimide-functionalized PFPA (PFPA-NHS) groups to generate surface azide groups, which were photoactivated for the covalent attachment of MIP nanoparticles.

The water contact angle measurements (Figure 4, **Paper I**) of the PFPA-treated surface before (80°) and after MIP immobilization (60°) showed a decrease in the hydrophobicity of the PFPA surface due to the immobilization of the –COOH-functionalized MIP particles. SEM images further confirm the successful MIP immobilization using PFPA-based photoconjugation (*cf.* Figure 4.1). Surface analysis of the surfaces prepared by each step was characterized using XPS. C 1s (Figure 3.3 (f)) and O 1s spectra (Figure 5, P**aper I**) show peak characteristic of the –COOH groups present on the MIP particles. The N 1s XP spectra (Figure 3.3 (c), P**aper I**) showed the disappearance of the azide peak on the PFPA surface after MIP immobilization, which is another strong confirmation of MIP photoconjugation.

Radioligand binding studies of the MIP surfaces showed that the imprinted particles retain their specificity compared to the non-imprinted polymer (NIP) surfaces. This proves the unaffected MIP binding properties after its photoconjugation on the support.

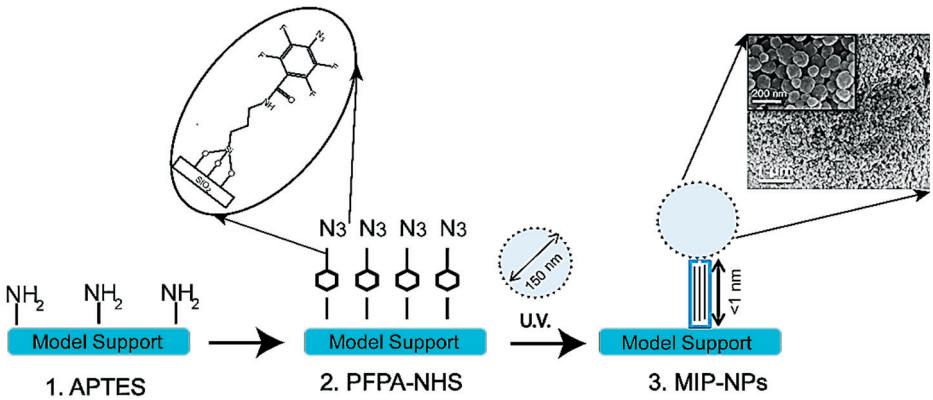

Figure 4.1. Scheme for the functionalization of APTES glass with PFPA-NHS followed by photoconjugation of MIP nanoparticles. An SEM micrograph shows the immobilized nanoparticles on the glass. Adapted from **Paper I**.

4.1.1.2 Epoxide ring opening reaction

Surface immobilization using epoxide chemistry is very well known for biomolecule attachment on solid surfaces through their amine groups. Epoxide functionalization of the organic and inorganic supports is quite easy, simple, and stable compared to functionalization using other functional groups. The epoxide ring on the solid surfaces undergo nucleophilic substitution by primary or secondary amine groups (-NH_2, -NH-), sulfydryl groups (-SH), or, less commonly, hydroxyl groups (-OH).[140] Silica or glass surfaces are functionalized by epoxy groups either using a silane coupling agent (GPTMS) or by coating with epoxy resins.

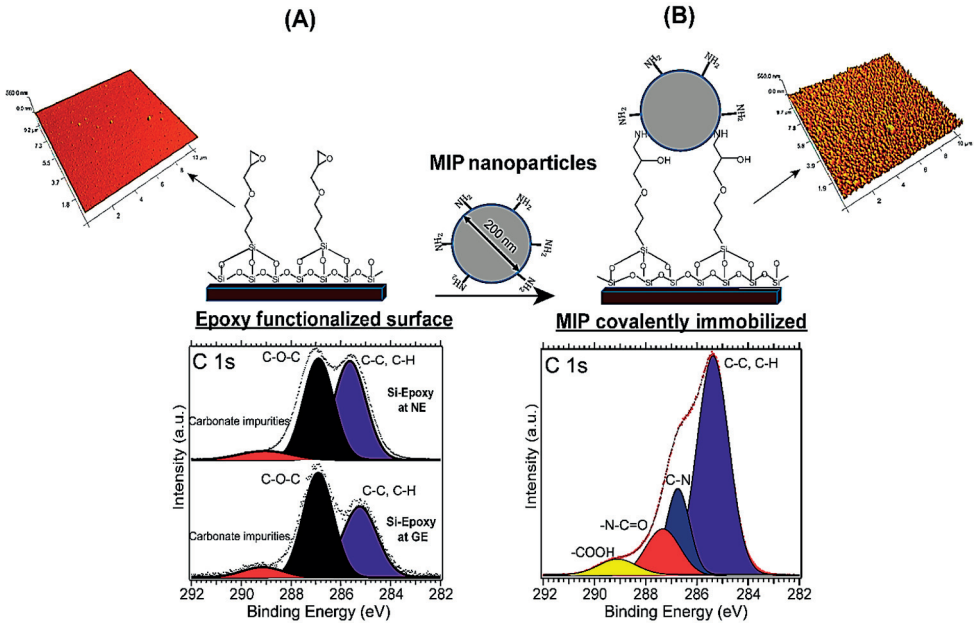

Figure 4.2. Scheme for MIP core-shell immobilization on an epoxide surface: (A) AFM image and C 1s XP spectra of the epoxy functionalized surface, and (B) AFM image and C 1s XP spectrum of the surface with immobilized MIP nanoparticles. Adapted from **Paper II**.

In this thesis, GPTMS is used to generate epoxy groups on glass and silicon wafers. The epoxy ring is stable at neutral pH, even in wet conditions. At basic pH, the epoxide ring opens and forms a covalent bond with the primary amines on the MIP core-shell nanoparticles. This results in a stable and homogenous MIP assembly on the solid support (Figure 4.2). The AFM images show the GPTMS or epoxy surface before and after MIP immobilization. The water contact angle measurements were also performed for the GPTMS surface before and after MIP immobilization. The water contact angle decreases from 55^{o} to 20^{o} between the GPTMS and MIP-on-GPTMS surfaces, i.e., after MIP immobilization (Figure S1, **Paper II**). This implies that the surface becomes hydrophilic in line with expectations: the MIP core-shell nanoparticles are hydrophilic due to the presence of the abundant amino groups in the shell. The fluorescent microscopy (Figure 3, **Paper II**) and SEM images (Figure S2, **Paper II**) further show the homogenous MIP assembly resulting from the epoxide ring opening reaction.

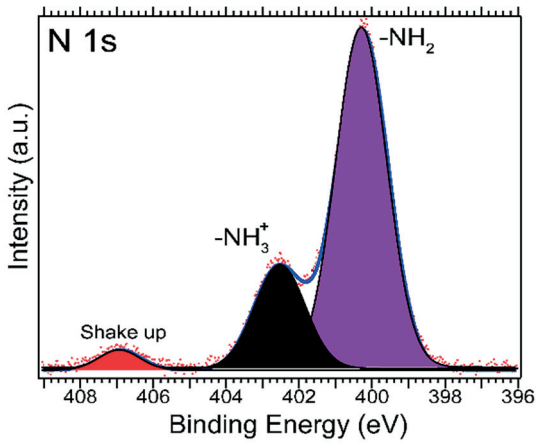

Figure 4.3. N 1s XP spectrum of covalently immobilized core-shell MIP nanoparticles on an epoxide surface. Adapted from **Paper II.**

It is possible to chemically analyze each functionalization step using XPS. In this thesis, I replaced the glass with a semiconducting silicon wafer due to the charging problems resulting from the insulating nature of the glass. Figure 4.2A shows the C 1s XP spectra of a GPTMS-functionalized silicon wafer (Si-Epoxy) with two prominent peaks due to the hydrocarbon and epoxide species. The increase in the intensity ratio of the epoxide peak to the hydrocarbon peak at the grazing emission (GE) compared to the normal emission (NE) further confirms the presence of the available surface for MIP immobilization. The C 1s (Figure 4.2B) and N 1s (Figure 4.3) spectra of the MIP immobilized silicon wafer (Si-Epoxy-MIP) show the peaks expected due to the presence of MIP core-shell particles.

To apply MIP-modified surfaces for chemical sensing, it is critical that the molecular selectivity of the immobilized MIP particles is not sacrificed during the conjugation reaction. In this work, I used autoradiography to verify that the chemical conjugation to the GPTMS-modified surface does not affect the interior binding sites of the core-shell MIP particles. In this technique, a radioactivity-sensitive photographic film is used. When brought into close contact with the radioisotope tritium (^{3}H), the film blackens, producing the image. Figure 4.4 shows the images obtained in the radioligand binding analysis. For the specificity of the MIP surface,

panel (B) shows a large contrast, compared to the blank silicon sample, panel (A), and the NIP surface, panel (C). The image intensity from the Si-Epoxy-MIP sample is eight times that of the Si sample and four times that of the Si-Epoxy-NIP sample, which clearly indicates that the MIP particles retain their high template affinity after chemical immobilization. To prove more clearly the molecular selectivity of Si-Epoxy-MIP, I performed competitive radioligand binding experiments on this surface by adding excess competitive compounds to the labeled propranolol solution. The three competitive compounds used are unlabeled propranolol, pindolol, and ANOP (*cf.* Figure 6, **Paper II**). As seen from Figure 4.4(D-G), the binding of the labeled propranolol to the Si-Epoxy-MIP sample decreased the most in the presence of the unlabeled propranolol compared to the other competing compounds, pindolol and ANOP. Collectively, the Si-Epoxy-MIP surface displays clear molecular selectivity, which can be attributed to the intact molecular binding sites located in the immobilized MIP particles.

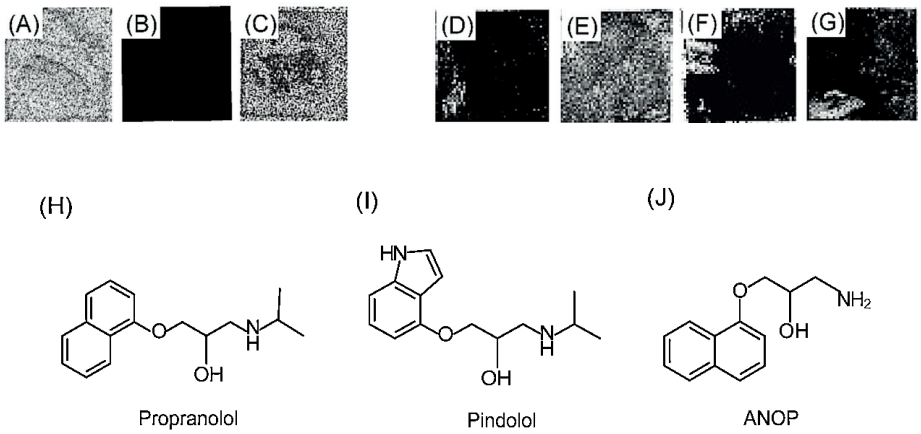

Figure 4.4. Autoradiography images showing the ^{3}H-labeled propranolol binding to three different surfaces: (A) Si, (B) Si-Epoxy-MIP and (C) Si-Epoxy-NIP. Autoradiography images showing ^{3}H-labeled propranolol binding to Si-Epoxy-MIP in the absence of a competing compound (D) and in the presence of 10 μM of propranolol (E), pindolol (F), and ANOP (G). Chemical structure of propranolol (H), pindolol (I), and ANOP (J). Adapted from **Paper II.**

4.1.1.3 Carbodiimide chemistry

Gold is usually selected as the surface material due to its chemical inertness, biocompatibility, and property that organic compounds can form well-ordered and packed monolayers on its surface.[141] Various thiol precursors have been used for surface functionalization of gold surfaces. The high affinity of thiols (R-SH), disulfides (R-S-S-R), and sulfides (R-S-R) for gold results in the formation of a well-ordered organic layer[142] with useful functional groups exposed on the surface for different sensor-based applications. The strong and fast adsorption of alkylthiolates requires a clean Au surface, which can be achieved by cleaning the Au surface in a highly oxidizing reagent, i.e., in either a piranha or electrochemical sulfuric acid solution or by ozone cleaning.[143] Film properties, such as structure and density of the resulting self-assembled monolayers (SAMs), can be affected by a number of factors, such as the solvent, temperature, concentration and purity of the adsorbate, the immersion time, and the concentration of oxygen in the solution.

Hetero-bifunctional thiol linkers are widely used due to their exposed surface groups, such as carboxyls (-COOH), which can be activated using the well-known carbodiimide chemistry[144] for covalent attachment of amino-functionalized molecules and nanomaterials (biomolecules, core-shell nanoparticles, etc.) on the Au surface. In **Paper IV**, 11-mercaptoundecanoic acid (MUA) was adsorbed on Au for covalent attachment of amino-functionalized MIP core-shell particles.

Figure 4.5 illustrates the approach used for the immobilization of MIP core-shell NPs. In this approach, the clean Au surface is functionalized with MUA to form a carboxyl-terminated surface followed by the EDC and NHS or carbodiimide activation. In the final step, the surface is exposed to a solution of propranolol-imprinted core-shell MIP particles to finish the covalent amide bond formation. The smooth and uniform underlying short-chain alkyl thiol MUA created –COOH-functionalized SAMs that are activated using EDC and NHS as the coupling reagents for MIP attachment. The succinimidyl ester generated by the NHS group finally reacted with the amine-functionalized MIP nanoparticles to form an amide bond.[145] The EDC/NHS activation decreases the energy barrier for carboxyl groups to react with the amino groups.

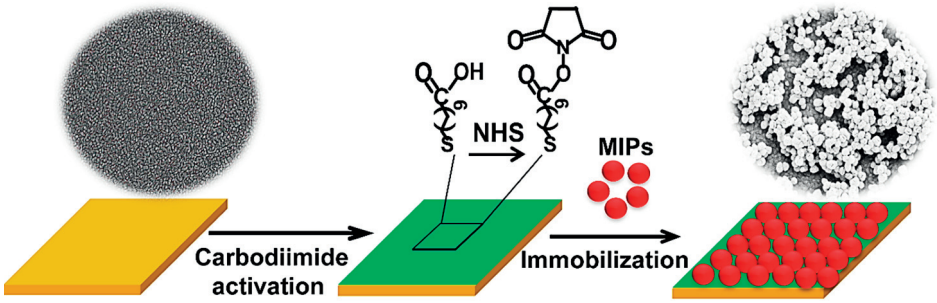

Figure 4.5. Scheme showing the immobilization of core-shell MIP nanoparticles on a gold surface using carbodiimide chemistry. SEM images shows the Au surface before and after MIP immobilization. Adapted from **Paper III.**

The change in surface contact angle (Figure 1, **Paper III**) proves the successful MUA functionalization (40°), activation (70°), and MIP immobilization (25°). The immobilized amine-functionalized MIP particles were made fluorescent after reaction with fluorescein isothiocyanate (FITC). A strong contrast in the fluorescent images (Figure S2, **Paper III**) proves the MIP immobilization. SEM and AFM images shows very few particles on the Au and Au@MUA control surface, as seen from Figures S1 and 2 in **Paper III.** In contrast, the density of the immobilized particles increased significantly after the EDC and NHS activation.

XPS measurements were performed at each step of immobilization. C 1s, N 1s, S 2p and O 1s lines were recorded for all four surfaces: (1) the clean Au (**Au**), (2) self-assembled MUA on Au (**Au@MUA**), (3) EDC and NHS-activated surface (**Au@NHS**), and (4) covalently immobilized MIP on the EDC and NHS activated surface (**Au@MIP**). Figure 4.6 compares each element of a surface and shows the presence of characteristic peaks or features of MIP particles. The appearance of the N 1s lines is attributed to successful activation of Au@MUA. The change in the N 1s lineshape after MIP immobilization confirms the removal of NHS and the attachment of amino group-functionalized MIP-NPs.

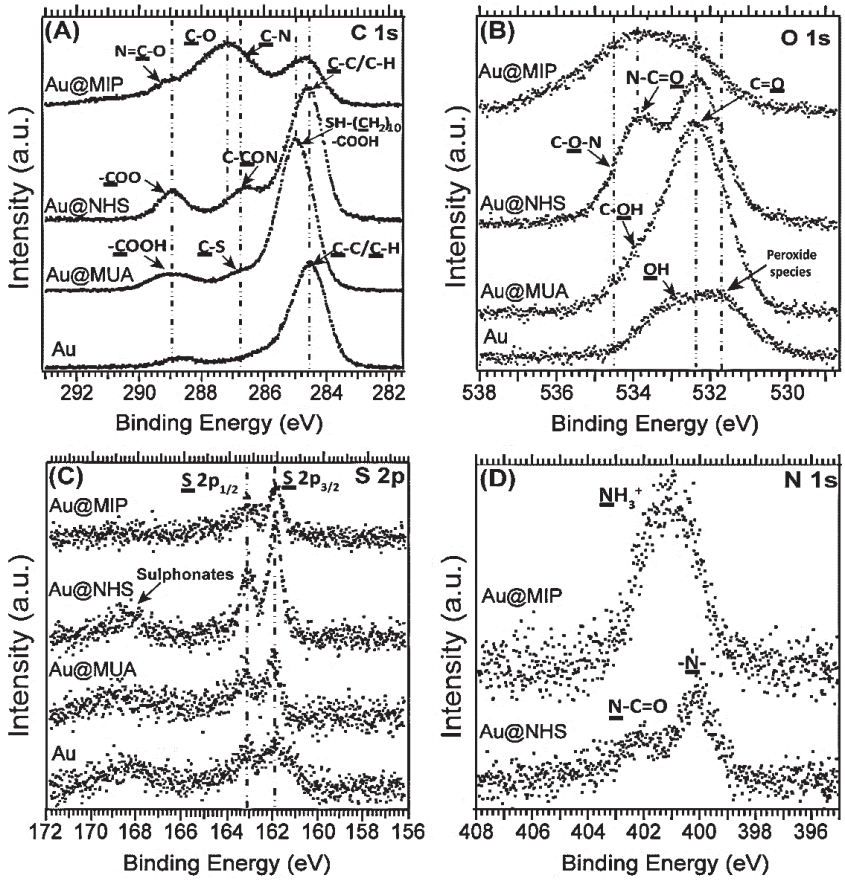

Figure 4.6. XP spectra obtained in normal emission geometry: (A) C 1s, (B) O 1s, and (C) S 2p of the clean Au, Au@MUA, Au@NHS, and Au@MIP surfaces, (D) N 1s of the Au@NHS activated surface and the Au@MIP surface. Photoemission is from the underlined atoms. Adapted from **Paper III.**

4.1.2. Electrostatic interaction using a polymer interlayer

In section 4.1.1, I reported different covalent approaches for MIP immobilization. It is interesting to study the MIP nanoparticles' immobilization using strong and long-range electrostatic interactions. These interactions can be either attractive or

repulsive depending on the charges of the two interacting objects. For this thesis, I used a positively charged interlayer of polymer for attaching negatively charged MIP nanoparticles to a solid glass substrate.

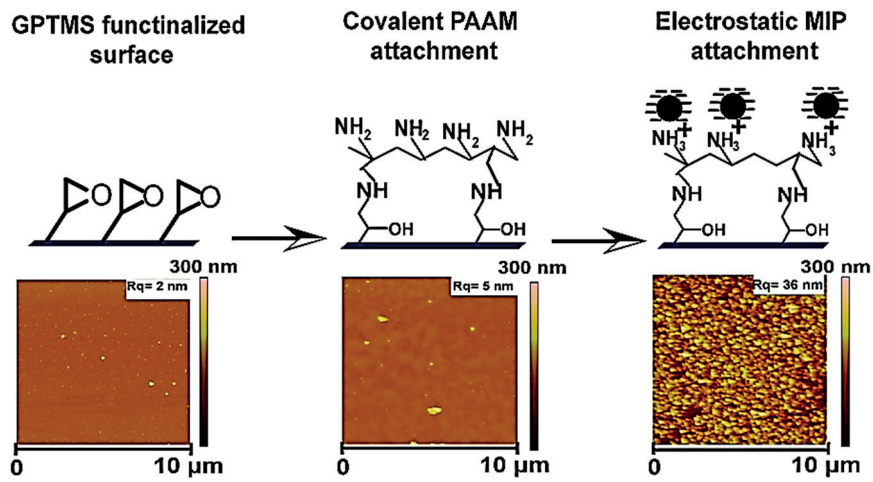

Figure 4.7. Steps involved for PAAm attachment on a GPTMS-functionalized surface followed by electrostatic MIP nanoparticle attachment. AFM images are shown for each surface, along with the change in their mean surface roughness Rq. Adapted from **Paper IV.**

In **Paper IV**, the grafting of an amino-functionalized polymer, polyallylamine (PAAm),[146] on an epoxy-modified glass surface is reported for the electrostatic attachment of the propranolol-imprinted MIP-NPs. PAAM contains a high content of primary amine functional groups and proves to be an efficient functional tool for the creation of a stable and homogenous MIP layer on a glass substrate. Figure 4.7 illustrates the approach used for immobilization of MIP nanoparticles, along with AFM images of each step. The uniform and stable GPTMS-functionalized surface contains reactive epoxide groups, and its exposure to the amine groups of the PAAm is expected to lead to a ring-opening reaction of the reactive three-membered epoxide ring to create a C-N bond.[147] The strong covalent attachment of the polymer is slow and irreversible. This generates multiple positively charged amino groups on the glass surface, which provides a large contact area and a large number of

anchor points for the negatively charged polymer spheres. Altogether, the scheme results in an electrostatic yet stable MIP layer on the solid support.

Contact angle measurements (Figure S1, **Paper IV**) clearly show the successful PAAm attachment and MIP immobilization on the glass support. The decrease in water contact angle from 65° for the GPTMS-modified to 40° on the PAAm surface confirms the attachment of the hydrophilic amino polymer on the hydrophobic epoxide surface.

SEM images in Figure S3 from the supporting information of **Paper IV** also show the change in the GPTMS-modified glass surface after PAAm attachment followed by dense MIP particle packing on the PAAm surface. I also recorded AFM images to learn more about the roughness and sectional profile (Figure S2, **Paper IV**) of the surfaces after each preparation step. The AFM images of the surfaces show the change in the surface morphology and the increase in roughness after PAAm and MIP attachment to the glass surface.

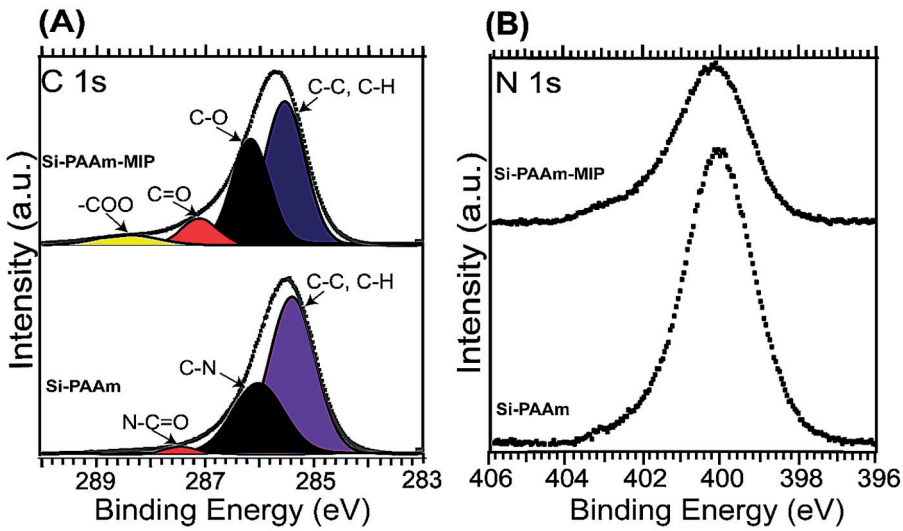

Figure 4.8. XP spectra: (A) C 1s and (B) N 1s of the Si-PAAm sample with the Si-PAAm-MIP sample measured in normal emission geometry. Adapted from **Paper IV.**

Additional confirmation of MIP electrostatic attachment on PAAm was verified by measurement of an XP spectra of a PAAm-coated silicon wafer (Si-PAAm) and the MIP-modified PAAm-coated silicon surface (Si-PAAm-MIP): overview spectra (Figure 2A, **Paper IV**), O 1s XP spectra (Figure 3, **Paper IV**), and C 1s and N 1s spectra (Figure 4.8). In Figure 4.8A, the C 1s line of Si-PAAm-MIP shows the presence of peaks at higher binding energy due to the –COOH groups of the MIP particles. However, the N 1s signal (Figure 4.8B) does not completely disappear, which indicates the presence of some PAAm areas left uncovered by MIP particles. The N 1s signal intensity decreases for the Si-PAAm-MIP surface, nonetheless providing attachment of MIP particles that shield the underlying PAAm.[148]

Template binding studies of the PAAm surfaces with conjugated MIP particles (Figure 4.9) show strong contrast for the Si-PAAm-MIP (C) compared to the blank (A), Si-PAAm (B), and Si-PAAm-NIP (D) surfaces, which shows that the PAAm conjugation does not affect the specificity of the MIP particles. The selectivity of the MIP surfaces is shown in the presence of other competing molecules, unlabeled propranolol (E), pindolol (G), and ANOP (H) (*cf.* Figure 4.4 (H-J)). As can be observed from Figure 4.9 (E-H), the Si-PAAm-MIP surface displays clear molecular selectivity, which can only be attributed to the intact molecular binding sites located in the immobilized MIP particles.

Figure 4.9. Autoradiography images showing the ^{3}H-labeled propranolol binding to four different surfaces: (A) Si, (B) Si-PAAm, (C) Si-PAAm-MIP, and (D) Si-PAAm-NIP. Autoradiography images showing ^{3}H-labeled propranolol binding to Si-PAAm-MIP in the absence of a competing compound (E) and in the presence of 10 μM of propranolol (F), pindolol (G), and ANOP (H). Adapted from **Paper IV.**

4.2. Surface-enhanced Raman spectroscopy sensors

The performance of a MIP sensor depends on (1) the stable and homogenous immobilization of the MIPs on the transducer surface, (2) the availability or accessibility of the template binding sites, and (3) the absence of interference due to the nonspecific adsorption on the solid transducer surface.

For the work in this thesis, I used covalent chemistry (Au-Thiol: **Paper V** and photoconjugation: **Paper VI**) to attach polymer spheres on solid surfaces and study their template binding property using the optical transduction method. Among the different optical sensing constructs, MIP sensors using SERS detection have become the most popular,[28-31] and portable Raman instruments are now available from many commercial vendors, with which detection can be carried out directly on both solid and liquid samples. The Raman signal from inelastic scattering, although characteristic for each analyte, is often very weak and difficult to detect. This problem of low sensitivity can be solved by depositing analytical samples on a roughened noble metal surface (e.g., silver or gold)[90-92] or on a metal-coated rough porous surface[29,94,95] that can generate localized surface plasmons upon light irradiation. The plasmon resonance is the basis for SERS.[86]

In my dissertation, *ex situ*-prepared MIP spheres were integrated on the transducer surface using approaches A and B in Figure 2.4 (Chapter 2). The MIP-loaded surfaces were then made Raman-active using both gold colloids as Raman enhancers and a SERS active surface (Klarite) for sensitive and selective detection of target analytes.

4.2.1. Nicotine detection

In **Paper V**, I designed an MIP-SH-based SERS sensor for the detection of nicotine. The thiol groups on the MIP surface allow the microspheres to be immobilized on a gold-coated substrate using the covalent Au-thiol interaction.[149] The SEM images in Figure 4.10 show a stable, dense, and homogenous coverage of the polymer sphere on solid Au. The preformed nicotine-imprinted polymer microspheres were

prepared as described in Chapter 2 (section 2.2.3).[66] Figure 4.10 also shows the three different strategies investigated to achieve surface-enhanced Raman scattering in the vicinity of the imprinted sites: (1) direct sputtering of gold nanoparticles, (2) immobilization of gold colloids through the MIP's thiol groups, and (3) trapping of the MIP microspheres in a patterned SERS substrate. For the first time, I showed that large MIP microspheres can be turned into selective SERS surfaces with sensitive and selective nicotine detection.

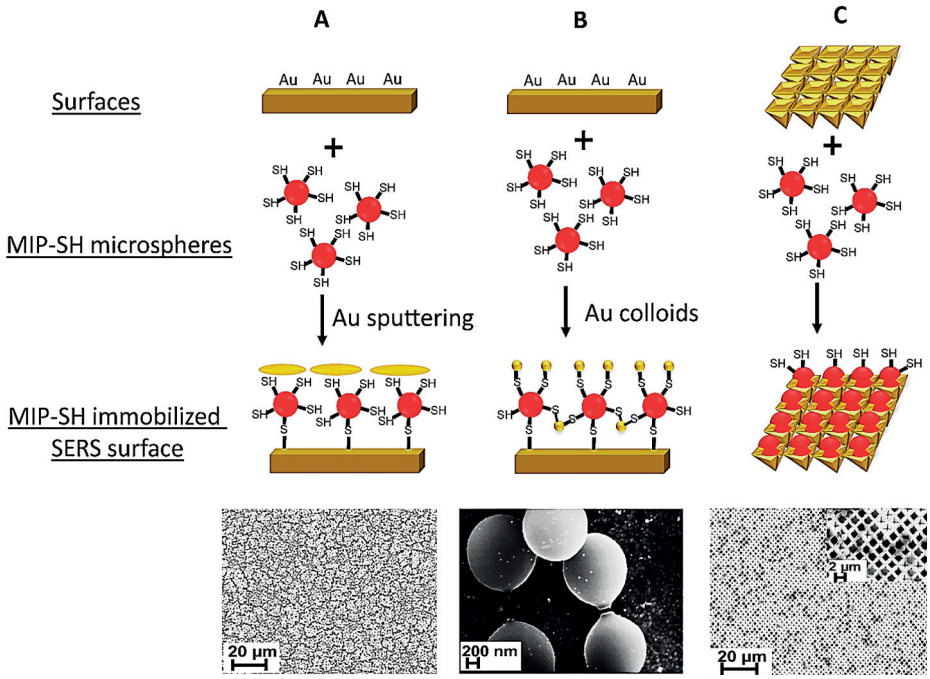

Figure 4.10. Three different approaches for SERS activation of MIP-SH microsphere surfaces for the detection of nicotine: (A) activation of the MIP surface by Au sputtering, (B) activation of the MIP surface using Au colloids (20 nm), and (C) activation of the MIP surface using the SERS-active Klarite surface. Adapted from **Paper V.**

In the ***first approach*** (Figure 4.10A), after the MIP-SH surface **(1)** sputter-coated with 5 nm of Au had been exposed to a nicotine solution, it generated the characteristic Raman signal at 1034 cm^{-1} **(2)**. Although the surfaces were Raman-

active and it was possible to detect the selective nicotine binding via the activated "hot spots," the detected Raman signal intensity does not increase further when the concentration of nicotine exceeds 30×10^{-5} M. This signifies that only the binding sites close to the particle surface can be utilized to give an effective signal response because the nicotine molecules bound in the interior of the particles are "invisible." Because the number of "visible" binding sites is limited, it is likely that these sites will be saturated at high nicotine concentrations.

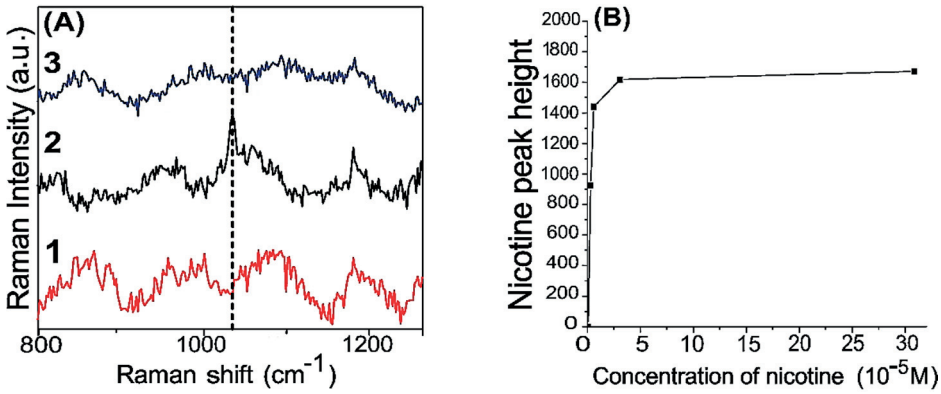

Figure 4.11. (A) Raman spectra collected from (1) an MIP surface after Au sputtering; (2) an MIP surface after Au sputtering and exposure to 6×10^{-5} M of nicotine; and (3) an NIP surface after Au sputtering and exposure to 6×10^{-5} M of nicotine. (B) Plot of Raman intensity vs. nicotine concentration, obtained using the activated MIP surface. Adapted from **Paper V.**

In the ***second approach*** (Figure 4.10B), the enhancement of the Raman signal is attributed to the plasmonic coupling between the surface-bonded Au colloids combined with the enriched nicotine molecules through their specific binding to the MIP-SH microspheres, resulting in local electromagnetic field enhancements. The MIP-SH surface showed a significant strong nicotine Raman peak compared to that of the NIP-SH, along with a linear response with the increase in nicotine concentration (Figure 4.12B). The selectivity of the MIP-SH surface was also studied in the presence of other competing molecules, propranolol and Rhodamine

B (**Paper V**, Figure 3D). Even in the presence of excess propranolol (characteristic band at 1385 cm^{-1})[150] and Rhodamine B (a basic and Raman active dye having a characteristic band at 1360 cm^{-1}),[151] the nicotine signal at 1034 cm^{-1} is still clearly visible.

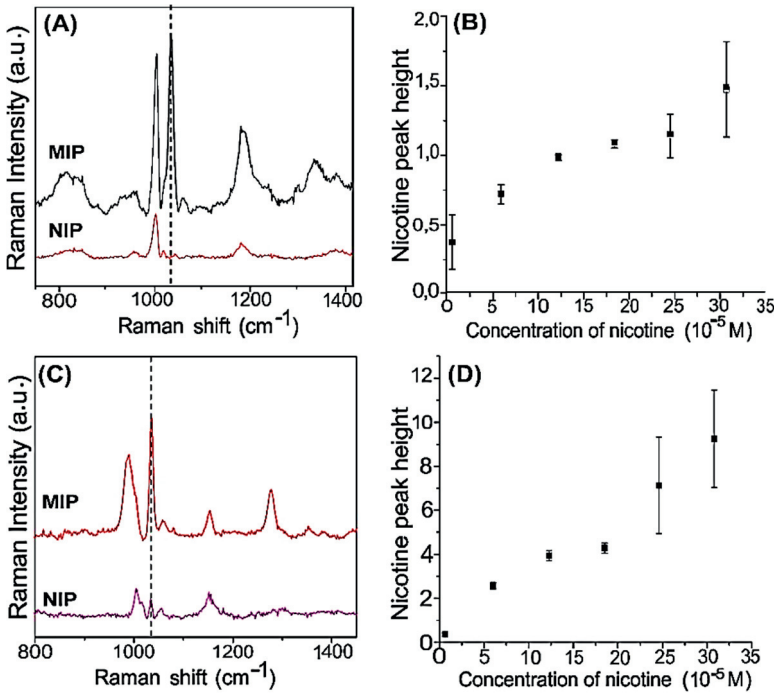

Figure 4.12. (A) Raman spectra of 30 × 10^{-5} M of nicotine (dotted line) obtained from MIP-SH and NIP-SH surfaces after deposition of Au colloids; (B) relative intensity of the normalized Raman band of nicotine at different concentrations; (C) Raman spectra of 6 × 10^{-5} M nicotine (dotted line) obtained from MIP-SH and NIP-SH loaded Klarite substrates; and (D) relative intensity of the normalized Raman band of nicotine at different concentrations. Adapted from **Paper V.**

In the ***third approach***, I studied the SERS of MIP-SH beads fitted inside the surface cavities of the Klarite substrate with no severe aggregation (*cf.* Figure 4.10). In Figure 4.12C, I observed a strong nicotine signal for the MIP-SH loaded Klarite surface (dotted line) compared to the NIP-SH surface. This proved the specificity of

the MIP-SH loaded Klarite, enabled by the binding with the SERS-enabling surface. Thus, MIP-SH loaded surfaces show good specificity with a linear response to a series of nicotine concentrations in the solution (Figure 4.12D). All three approaches can be used for detecting nicotine efficiently, but the ***second*** and ***third*** proved to be highly sensitive towards the template molecule.

4.2.2. Propranolol detection

In **Paper VI**, I reported another interesting SERS-based MIP sensor for the real-time detection of propranolol. Although detection of β-blockers in urine has been reported earlier using MIPs as solid phase extraction sorbents[152,153] and MIPs as room temperature phosphorescent sensors,[154] these methods are tedious, time-consuming and difficult to use for on-site sample analysis. The simple and compact SERS system studied in this work is used as a model to demonstrate the general applicability of the reported construction method.

In this approach, I used the PFPA-based photoconjugation method for direct immobilization of MIP nanoparticles on a highly Raman-active substrate (Klarite). The hetero-bifunctional PFPA-disulfide has an alkyl chain of 11 carbons (PFPA-C_{11}-S)$_2$. The disulfide group forms stable bonds with the gold coated on the Klarite substrate. The exposed azide group was used to form covalent bonds with the MIP nanoparticles upon UV activation (Figure 4.13).

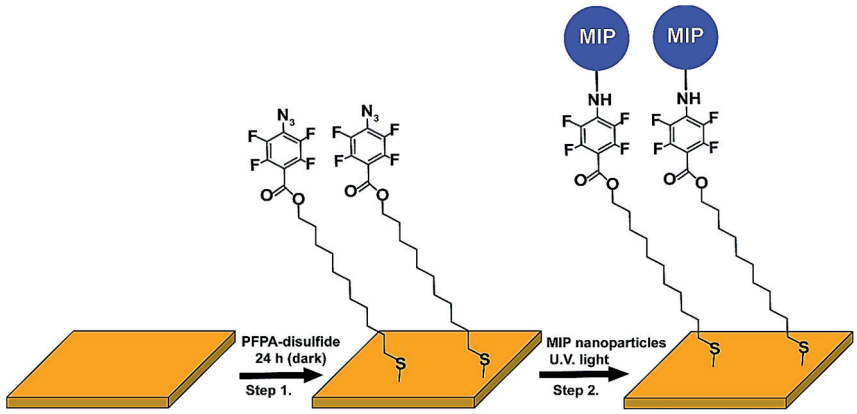

Figure 4.13. Immobilization of MIP nanoparticles on a PFPA-functionalized Klarite surface using photoconjugation chemistry. **Step 1**: functionalization of Klarite with PFPA-disulfide, **Step 2**: photoconjugation of MIP nanoparticles on PFPA-functionalized Klarite. Adapted from **Paper VI**.

Figures 4.14A and C show the SEM images of the Klarite surfaces after MIP and NIP particle attachment. The particles were packed in the patterned cavities on the Klarite substrate and could withstand repeated washing steps. Figure 4.14B shows the regenerated MIP particle surfaces with particles still attached inside the Klarite cavities. The MIP-coated substrate was tested as a Raman-active surface to detect propranolol at different concentrations. The characteristic Raman band at 1385 cm^{-1} due to the naphthalene moiety of the propranolol molecule[150] starts to appear when the propranolol concentration reaches 38×10^{-6} M (*cf.* Figure 2A, **Paper VI**). This shows the sensitivity of the MIP-based Raman sensor for detecting propranolol at low concentrations. The NIP-coated Klarite produced a much weaker propranolol signal due to the lack of high affinity sites for propranolol (*cf.* Figure 2B, **Paper VI**).

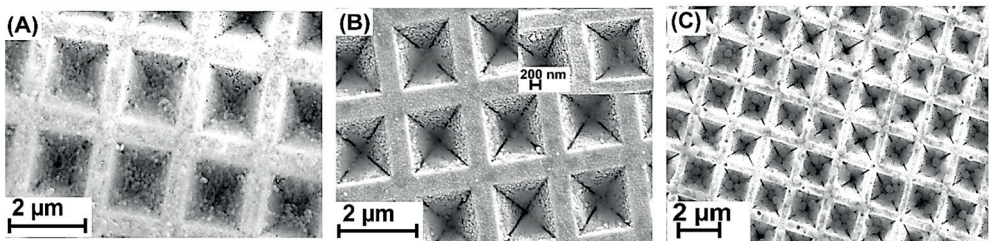

Figure 4.14. SEM images of (A) MIP nanoparticles photoconjugated to PFPA-functionalized Klarite; (B) MIP nanoparticles photoconjugated on PFPA-functionalized Klarite, regenerated by washing with acetic acid; and (C) NIP nanoparticles photoconjugated on PFPA-functionalized Klarite. Adapted from **Paper VI**.

A dose-response propranolol curve for the MIP- and the NIP-coated Klarite (Figure 4.15A) was obtained. Obviously, the MIP-coated Klarite produced a significantly higher analytical signal than the NIP-coated Klarite. To test the reusability of the MIP-coated substrate, I also tried to regenerate the sensing surface by washing the MIP-coated substrate in an acetic acid solution. From Figure 3A in **Paper VI**, it can be seen that, after the bound, propranolol was eluted from the MIP surface, the Raman band at 1385 cm^{-1} disappeared. This band appears again after the regenerated MIP surface was exposed to the same propranolol solution.

To detect the propranolol in a urine sample, the MIP-coated Klarite was incubated in the sample. Figure 4.15B shows the results of the SERS measurements with a sharp peak at 1003 cm^{-1} caused by the C-N stretching in the area that was abundant in urine.[155] As observed from the spectra, the MIP-coated Klarite allowed propranolol detection at a concentration of 77×10^{-5} M (curve 5). In contrast to the MIP-coated surface, neither the Klarite alone (curve 1) nor the NIP-coated Klarite (curve 4) gave any detectable propranolol signal under the same condition. Therefore, it can be concluded that only the MIP-coated Klarite can act as a useful sensing surface to measure propranolol in the complex urine sample.

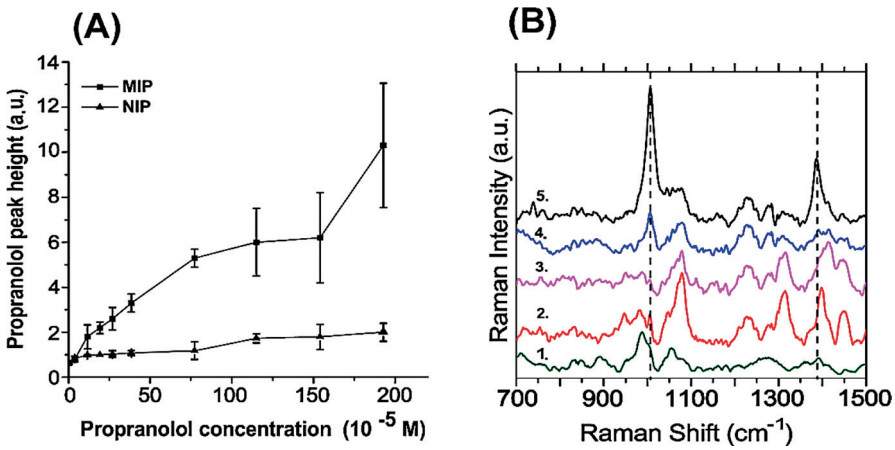

Figure 4.15. (A) Normalized intensity of the propranolol signal (1385 cm^{-1}) measured using the MIP- and the NIP-coated substrates. (B) Detection of propranolol in urine samples. Raman spectra of (1) urine spiked with 77×10^{-5} M propranolol measured on a Klarite substrate, (2) MIP-coated Klarite, (3) NIP-coated Klarite, (4) urine spiked with 77×10^{-5} M propranolol measured on the NIP-coated Klarite substrate, and (5) urine spiked with 77×10^{-5} M propranolol measured on the MIP-coated Klarite substrate. Adapted from **Paper VI**.

5. Conclusions and Future outlook

Conclusions

In recent years, different MIP-based sensors and other functional materials that are replacing the time-consuming and unstable (physical and chemical) chemical biosensors have been reported. The major problem associated with MIP sensors is that perfect conjugation with the transducer is required, which does not affect their analyte binding sites. The main goal of my PhD research was to integrate pre-made functional imprinted polymer particles or spheres on different solid surfaces and implement the obtained surfaces for real-time sensing of drugs and toxic materials in biological samples.

In the first part of my thesis (**Papers I-IV**), I reported different possible MIP immobilization chemistries on model substrates (glass, silicon, and Au wafers). The functional linkers generated on the substrates help to interact with the functionalities on the imprinted polymer spheres, resulting in either covalent or electrostatic immobilization. First, ***covalent*** assembly of MIP particles was studied. In **Paper I**, the photoconjugation method was reported to attach propranolol-imprinted MIP particles to a glass surface. This short coupling agent can be used to couple organic materials for the development of various functional nanomaterials. In **Paper II**, the amino-functionalized core-shell MIP nanoparticles were immobilized on a glass substrate using an epoxy silane linker. The amine groups on the MIP surface proved to be highly efficient for an opening epoxide ring reaction, which enables attachment of the MIP particles covalently on a solid surface. An important feature of this method is its versatility for the homogeneous and covalent immobilization of even materials with a relatively large size. The coupling reaction is easy, reproducible, and efficient without affecting the specificity and molecular recognition properties of the MIP nanoparticles. The approach does not require high temperature or photo- or chemical activation, which renders the method physically

and chemically more robust and useful in comparison to other immobilization procedures.

The reported covalent approach was studied on the silica and glass substrates, but for many sensor applications, one needs a metal transducer surface. Gold is a suitable candidate due to its stability in different chemical environments and its outstanding optical and electrical properties. This made me interested in studying the covalent immobilization of propranolol-imprinted core-shell nanoparticles on an Au surface (**Paper III)** instead of glass/silica (**Paper II**). Au was functionalized with a self-assembled monolayer of thiols. The thiol linkers on Au were activated using carbodiimide chemistry and proved successful for stable and high-density MIP immobilization. Further confirmation of EDC/NHS activation and subsequent MIP attachment on the EDC/NHS surface was conducted using XPS chemical analysis.

In addition to studying these covalent approaches for MIP-NP immobilization on solid supports, I also studied ***electrostatic*** MIP attachment. The negatively charged soft polymer spheres were attached to a positively charged polymer interlayer via strong electrostatic interactions. The electrostatic attachment proved to be a robust, easy, and fast approach for stable immobilization of MIP nanoparticles on a solid substrate. The method allows solid materials of submicron size to be immobilized on a surface with high density using a "soft" cationic polymer interlayer.

Not much work has been reported in the literature on the use of chemically immobilized MIP spheres for SERS studies. This lack of research motivated me to proceed in the sensing direction and thus to the work presented in the second part of my thesis. I carried out SERS-sensing studies of propranolol and nicotine using MIP spheres. Integration of the immobilized MIP spheres on Au wafers with pre-synthesized Au colloids helped in enhancing the nicotine Raman signal (**Paper V**). Both dose-responsive and competition studies examined the concentration dependence and the selectivity of the sensor. Additional studies were also performed for the detection of propranolol in a complex biological sample using SERS (**Paper VI**). The covalent attachment of the nanoparticles on the Raman-active surface was achieved using straightforward photoconjugation. The photoconjugation method to integrate MIP with the Raman substrate is simple, robust, and sensitive for propranolol detection.

Future outlook

In my research studies, I concluded different immobilization chemistries for the attachment of MIP nanoparticles (100-300 nm) and microspheres (2 μm) to inorganic surfaces. Further work should be carried out to study the immobilization of other functionalized MIP spheres (varying sizes) on different metal transducer surfaces and use the array of particles for the extraction of different microbes, toxins, and gases from the environment, food products and biological fluids (blood, serum, etc.)

I believe that the MIP spheres have excellent template-binding properties and, if conjugated with functional nanoparticles (other than gold) such as silver, quantum dots and TiO_2, can result in highly efficient SERS-functional materials suitable for chemical and biosensing applications. The Klarite surface used in the propranolol SERS studies can be replaced by other Raman-active surfaces, e.g., porous alumina membranes with a gold coating.[93] I believe that, by using smaller MIP nanoparticles in combination with better-controlled nanoparticle deposition, MIP-based SERS surfaces can be obtained with more precise control and that the analytical performance of such sensing elements can be improved significantly to satisfy practical applications. The MIP spheres can be imprinted against other biomolecules, microorganisms, etc. which makes them suitable for the development of various functional biomaterials and composites for chromatography, assays, and catalysis applications. Moreover, MIP particles could be patterned on electrodes using NanoImprint lithography and microfluidic techniques to fabricate more advanced MEMS sensors.

Acknowledgement

I would like to express my gratitude to my supervisors **Lei Ye**, **Joachim Schnadt** and **Lars Montelius** for giving me an opportunity to work in their groups and the continuous support and guidance during the whole process. Also I am very appreciative to my supervisor Lei's unspoken open door policy which meant that I could go to his office any time of the day and he solved my problems and guide me throughout my work. Many thanks to Achim for teaching me the important concepts of physics and making me confident to manage lot of other important things independently and efficiently. I would like to acknowledge **Stacey Ristinmaa Sorensen**, **Johan Gustafson** and **Anneli Nilsson Ahlm** for helping in all the official matters and support I needed in the physics department. In chemistry department, I would like to give my special thanks to **Professor Leif Bülow**, **Professor Per-Olof Larsson**, **Ulla Jeppsson Wistrand**, and **Docent Estera Dey** for their suggestions, support and enormous healthy discussions during fika and other times.

I thank all my colleagues in both physics and chemistry department for their overwhelming support and help in my research, especially **Changgang Xu, Xiantao Shen, Tongchang Zhou, Shilpi Chaudhary, Payam Shayesteh, Olesia Snezhkova and Niclas Johansson.**

A very special thanks to my office mate and a very dear friend **Dr. Hans-Olof Johansson** for all the help and short talks in between the writing. His presence in the office gave a very nice company and someone to talk to whenever I felt alone during the day.

A humble thanks to the people in Lund Nano Lab- **Ivan Maximov** for allowing me work in nanolab, **Håkan Lapovski**, **Peter Blomqvist, Anders Kvennefors, Mariusz Graczyk**, and **George Rydnemalm** for training and helping me in the characterization tools used in this thesis.

I want to acknowledge **Patrik Wirgin** for his great help in all my travelling bills and other non-work related official documentation.

Many thanks to **Sheetal Sisodiya** for the discussions and funny talks we had in lunch breaks along with the memorable weekends and spring excursions. Furthermore, I would thanks to all my friends in Lund especially **Devika Mehra, Sandeep Chakane, Tania Singh, Vaibhav Diwan, Jneshwari Malik, Priya Verma**, **Gunjan Verma**, **Ekaterina Bolbat, Mario Grossi, and Maitham Majeed** for your love, support, care and concern.

To all my friends in different parts of Europe and UK for their phone calls, messages and concern. This means a lot to me and without you guys it would have been difficult

Cedric Dicko, thanks for introducing me to your Raman set up and solving all the problems I faced during my experiments.

Thanks to **Sofie Elmorth** for allowing me to use the autoradiography instrument and **Alak Alshiekh** for help and training in using the instrument.

Sorry if I forget to mention other names. Many thanks to you as well.

Finally I would like to thank my family and well-wishers for their endless support thorough out my entire PhD journey. Their voices of encouragement and support motivated me to continue on my path firmly. I would like to dedicate this thesis to my father **Raj Kumar Kamra** and **Jaishree Kamra** my brother **Manish Kamra** for their never ending patience and words of wisdom throughout my life. Special thanks to my mother, **Jaishree Kamra** for being a guide and a best friend and this thesis is dedicated to you as you always wanted me to be a doctor and touch new heights in my life. Love u mom truly and deeply forever. I miss you a lot here.

References

(1) Zhao, Y. S.; Fu, H.; Peng, A.; Ma, Y.; Xiao, D.; Yao, J. Low-dimensional nanomaterials based on small organic molecules: Preparation and optoelectronic properties.*Adv. Mater.* 2008, *20*, 2859-2876.

(2) Alivisatos, P. The use of nanocrystals in biological detection.*Nat. Biotechnol.* 2004, *22*, 47-52.

(3) Atwater, H. A.; Polman, A. Plasmonics for improved photovoltaic devices.*Nat. Mater.* 2010, *9*, 205-213.

(4) Hu, J.; Odom, T. W.; Lieber, C. M. Chemistry and Physics in One Dimension: Synthesis and Properties of Nanowires and Nanotubes.*Acc. Chem. Res*. 1999, *32*, 435-445.

(5) Katz, E.; Willner, I. Integrated Nanoparticle–Biomolecule Hybrid Systems: Synthesis, Properties, and Applications.*Angew. Chem. Int. Ed.* 2004, *43*, 6042-6108.

(6) Yin, Y.; Alivisatos, A. P. Colloidal nanocrystal synthesis and the organic-inorganic interface.*Nature* 2005, *437*, 664-670.

(7) Padmanabhan, S. C.; Linehan, K.; O'Brien, S.; Kassim, S.; Doyle, H.; Povey, I. M.; Schmidt, M.; Pemble, M. E. A bottom-up fabrication method for the production of visible light active photonic crystals.*J. Mater. Chem. C* 2014, *2*, 1675-1682.

(8) Xiang, J. H.; Zhu, P. X.; Masuda, Y.; Okuya, M.; Kaneko, S.; Koumoto, K. Flexible solar-cell from zinc oxide nanocrystalline sheets self-assembled by an in-situ electrodeposition process.*J. Nanosci. Nanotechnol.* 2006, *6*, 1797-1801.

(9) Wang, X.; Zhi, L.; Müllen, K. Transparent, Conductive Graphene Electrodes for Dye-Sensitized Solar Cells.*Nano Lett.* 2008, *8*, 323-327.

(10) Mascolo, D.; Pascale, E.; Petrone, I.; Vecchione, R.; Volpe, M. V.; Malagnino, N.; Ruggiero, D.; Foncellino, F.; Bevilacqua, M. F.; Di Palma, V.; Cimmino, A.; Casuscelli, V.; Scaldaferri, R.; Pedaci, I.; Di Matteo, A.; Napolitano, T.; Salzillo, G.; Porro, F.; Maglione, M. G.; Occhipinti, L. Printed functionalized capacitors for water-induced label-free detection of DNA hybridization.*Sci. Adv. Mater.* 2011, *3*, 496-514.

(11) Holewinski, A.; Xin, H.; Nikolla, E.; Linic, S. Identifying optimal active sites for heterogeneous catalysis by metal alloys based on molecular descriptors and electronic structure engineering.*Curr. Opin. Chem. Eng.* 2013, *2*, 312-319.

(12) Akdim, O.; Demirci, U. B.; Miele, P. A bottom-up approach to prepare cobalt-based bimetallic supported catalysts for hydrolysis of ammonia borane.*Int. J. Hydrogen Energy* 2013, *38*, 5627-5637.

(13) Shen, Q.; Jiang, L.; Zhang, H.; Min, Q.; Hou, W.; Zhu, J. J. Three-dimensional dendritic Pt nanostructures: Sonoelectrochemical synthesis and electrochemical applications.*J. Phys. Chem. C* 2008, *112*, 16385-16392.

(14) Ting, Z.; Syed, M.; Nosang, V. M.; Marc, A. D. Recent progress in carbon nanotube-based gas sensors.*Nanotechnology* 2008, *19*, 332001.

(15) Welsher, K.; McManus, S. A.; Hsia, C. H.; Yin, S.; Yang, H. Discovery of protein- and DNA-imperceptible nanoparticle hard coating using gel-based reaction tuning.*J. Am. Chem. Soc*. 2015, *137*, 580-583.

(16) Coluccio, M. L.; Gentile, F.; Francardi, M.; Perozziello, G.; Malara, N.; Candeloro, P.; Di Fabrizio, E. Electroless deposition and nanolithography can control the formation of materials at the nano-scale for plasmonic applications.*Sensors (Switzerland)* 2014, *14*, 6056-6083.

(17) Weiler, M.; Quint, S. B.; Klenk, S.; Pacholski, C. Bottom-up fabrication of nanohole arrays loaded with gold nanoparticles: extraordinary plasmonic sensors.*Chem. Commun.* 2014, *50*, 15419-15422.

(18) Pal, T.; Narayanan, V. A.; Stokes, D. L.; Vo-Dinh, T. Surface-enhanced Raman detection of nicotinamide in vitamin tablets.*Anal. Chim. Acta* 1998, *368*, 21-28.

(19) Ye, S.; Wu, Y.; Zhang, W.; Li, N.; Tang, B. A sensitive SERS assay for detecting proteins and nucleic acids using a triple-helix molecular switch for cascade signal amplification.*Chem. Commun.* 2014, *50*, 9409-9412.

(20) Ruigrok, V. J. B.; Levisson, M.; Eppink, M. H. M.; Smidt, H.; van der Oost, J. Alternative affinity tools: more attractive than antibodies?*Biochem. J* 2011, *436*, 1-13.

(21) Cheong, W. J.; Yang, S. H.; Ali, F. Molecular imprinted polymers for separation science: A review of reviews.*J. Sep. Sci.* 2013, *36*, 609-628.

(22) Haupt, K.; Mosbach, K. Molecularly imprinted polymers and their use in biomimetic sensors.*Chem. Rev.* 2000, *100*, 2495-2504.

(23) Zhang, Q.; Jing, L.; Wang, Y.; Zhang, J.; Ren, Y.; Wang, Y.; Wei, T.; Liedberg, B. Surface plasmon resonance sensor for femtomolar detection of testosterone with water-compatible macroporous molecularly imprinted film.*Anal. Biochem.* 2014, *463*, 7-14.

(24) Kolarov, F.; Niedergall, K.; Bach, M.; Tovar, G. E. M.; Gauglitz, G. Optical sensors with molecularly imprinted nanospheres: A promising approach for robust and label-free detection of small molecules.*Anal. Bioanal. Chem*. 2012, *402*, 3245-3252.

(25) Walker, N. R.; Linman, M. J.; Timmers, M. M.; Dean, S. L.; Burkett, C. M.; Lloyd, J. A.; Keelor, J. D.; Baughman, B. M.; Edmiston, P. L. Selective detection of gas-phase TNT by integrated optical waveguide spectrometry using molecularly imprinted sol-gel sensing films.*Anal. Chim. Acta* 2007, *593*, 82-91.

(26) Das, K.; Penelle, J.; Rotello, V. M. Selective picomolar detection of hexachlorobenzene in water using a quartz crystal microbalance coated with a molecularly imprinted polymer thin film.*Langmuir* 2003, *19*, 3921-3925.

(27) Jakusch, M.; Janotta, M.; Mizaikoff, B.; Mosbach, K.; Haupt, K. Molecularly imprinted polymers and infrared evanescent wave spectroscopy. A chemical sensors approach.*Anal. Chem.* 1999, *71*, 4786-4791.

(28) Kantarovich, K.; Tsarfati, I.; Gheber, L. A.; Haupt, K.; Bar, I. Reading microdots of a molecularly imprinted polymer by surface-enhanced Raman spectroscopy.*Biosens. Bioelectron.* 2010, *26*, 809-814.

(29) Bompart, M.; De Wilde, Y.; Haupt, K. Chemical nanosensors based on composite molecularly imprinted polymer particles and surface-enhanced Raman scattering.*Adv. Mater.* 2010, *22*, 2343-2348.

(30) Holthoff, E. L.; Stratis-Cullum, D. N.; Hankus, M. E. A Nanosensor for TNT Detection Based on Molecularly Imprinted Polymers and Surface Enhanced Raman Scattering.*Sensors-Basel* 2011, *11*, 2700-2714.

(31) Liu, P.; Liu, R. Y.; Guan, G. J.; Jiang, C. L.; Wang, S. H.; Zhang, Z. P. Surface-enhanced Raman scattering sensor for theophylline determination by molecular imprinting on silver nanoparticles.*The Analyst* 2011, *136*, 4152-4158.

(32) Marazuela, M.; Moreno-Bondi, M. Fiber-optic biosensors – an overview.*Anal. Bioanal. Chem*. 2002, *372*, 664-682.

(33) Ye, L.; Mosbach, K. Molecular Imprinting: Synthetic Materials As Substitutes for Biological Antibodies and Receptors.*Chem. Mater*. 2008, *20*, 859-868.

(34) Alexander, C.; Andersson, H. S.; Andersson, L. I.; Ansell, R. J.; Kirsch, N.; Nicholls, I. A.; O'Mahony, J.; Whitcombe, M. J. Molecular imprinting science and technology: a survey of the literature for the years up to and including 2003.*J. Mol. Recogn.* 2006, *19*, 106-180.

(35) Whitcombe, M. J.; Alexander, C.; Vulfson, E. N. Smart polymers for the food industry.*Trends Food Sci. Technol.* 1997, *8*, 140-145.

(36) Ramstrom, O.; Ye, L.; Mosbach, K. Artificial antibodies to corticosteroids prepared by molecular imprinting.*Chem. Biol*. 1996, *3*, 471-477.

(37) Wulff, G.; Sarhan, A. Use of Polymers with Enzyme-Analogous Structures for Resolution of Racemates.*Angew. Chem. Int. Ed.* 1972, *11*, 341-&.

(38) Ansell, R. J.; Kriz, D.; Mosbach, K. Molecularly imprinted polymers for bioanalysis: Chromatography, binding assays and biomimetic sensors.*Curr. Opin. Biotechnol.* 1996, *7*, 89-94.

(39) Mosbach, K.; Ramstrom, O. The emerging technique of molecular imprinting and its future impact on biotechnology.*Bio-Technol.* 1996, *14*, 163-170.

(40) Polyakov, M. V. Adsorption properties and structure of silica gel *Zhurnal Fizieskoj Khimii/Akademiya SSSR* 1931, *2*, 799-805.

(41) Wei, S.; Jakusch, M.; Mizaikoff, B. Capturing molecules with templated materials—Analysis and rational design of molecularly imprinted polymers.*Anal. Chim. Acta* 2006, *578*, 50-58.

(42) Wulff, G. Molecular Imprinting in Cross-Linked Materials with the Aid of Molecular Templates - a Way Towards Artificial Antibodies.*Angew. Chemi. Int. Ed.* 1995, *34*, 1812-1832.

(43) Maier, N. M.; Lindner, W. Chiral recognition applications of molecularly imprinted polymers: a critical review.*Anal. Bioanal. Chem*. 2007, *389*, 377-397.

(44) Whitcombe, M. J.; Rodriguez, M. E.; Villar, P.; Vulfson, E. N. A new method for the introduction of recognition site functionality into polymers prepared by molecular imprinting: Synthesis and characterization of polymeric receptors for cholesterol.*J. Am. Chem. Soc*. 1995, *117*, 7105-7111.

(45) Ye, L.; Springer Berlin Heidelberg, 2015, pp 1-24.

(46) Chen, L. X.; Xu, S. F.; Li, J. H. Recent advances in molecular imprinting technology: current status, challenges and highlighted applications.*Chem. Soc. Rev.* 2011, *40*, 2922-2942.

(47) Li, Z.; Ding, J.; Day, M.; Tao, Y. Molecularly Imprinted Polymeric Nanospheres by Diblock Copolymer Self-Assembly.*Macromolecules* 2006, *39*, 2629-2636.

(48) Poma, A.; Turner, A. P. F.; Piletsky, S. A. Advances in the manufacture of MIP nanoparticles.*Trends Biotechnol*. 2010, *28*, 629-637.

(49) Vasapollo, G.; Del Sole, R.; Mergola, L.; Lazzoi, M. R.; Scardino, A.; Scorrano, S.; Mele, G. Molecularly Imprinted Polymers: Present and Future Prospective.*Int. J. Mol. Sci*. 2011, *12*, 5908-5945.

(50) Ye, L.; Cormack, P. A. G.; Mosbach, K. Molecularly imprinted monodisperse microspheres for competitive radioassay.*Anal. Commun.* 1999, *36*, 35-38.

(51) Ye, L.; Weiss, R.; Mosbach, K. Synthesis and characterization of molecularly imprinted microspheres.*Macromolecules* 2000, *33*, 8239-8245.

(52) Yoshimatsu, K.; Reimhult, K.; Krozer, A.; Mosbach, K.; Sode, K.; Ye, L. Uniform molecularly imprinted microspheres and nanoparticles prepared by

precipitation polymerization: The control of particle size suitable for different analytical applications.*Anal. Chim. Acta* 2007, *584*, 112-121.

(53) Eshuis, A.; Leendertse, H. J.; Thoenes, D. Surfactant-free emulsion polymerization of styrene using crosslinked seed particles.*Colloid. Polym. Sci.* 1991, *269*, 1086-1089.

(54) Tamai, H.; Nishida, Y.; Suzawa, T. Surface properties of micron-size polystyrene latex particles prepared by seeded polymerization.*J. Colloid. Interface Sci*. 1991, *146*, 288-290.

(55) Bon, S. A. F.; Van Beek, H.; Piet, P.; German, A. L. Emulsifier-free synthesis of monodisperse core-shell polymer colloids containing chloromethyl groups.*Journal of Applied Polymer Science* 1995, *58*, 19-29.

(56) Kawaguchi, S.; Yekta, A.; Winnik, M. A. Surface Characterization and Dissociation Properties of Carboxylic Acid Core–Shell Latex Particle by Potentiometric and Conductometric Titration.*J Colloid Interface Sci*. 1995, *176*, 362-369.

(57) Okubo, M.; Lu, Y. Preparation of heterogeneous film from core-shell composite polymer particles produced by the stepwise heterocoagulation method with heat treatment.*Colloid. Polym. Sci*. 1996, *274*, 1020-1024.

(58) Okubo, M.; Lu, Y. Production of core-shell composite polymer particles utilizing the stepwise heterocoagulation method.*Colloids Surf., A* 1996, *109*, 49-53.

(59) Pérez, N.; Whitcombe, M. J.; Vulfson, E. N. Molecularly imprinted nanoparticles prepared by core-shell emulsion polymerization.*J. Appl. Polym. Sc.* 2000, *77*, 1851-1859.

(60) Pérez-Moral, N.; Mayes, A. G. Noncovalent Imprinting in the Shell of Core-Shell Nanoparticles.*Langmuir* 2004, *20*, 3775-3779.

(61) Hajizadeh, S.; Xu, C. G.; Kirsebom, H.; Ye, L.; Mattiasson, B. Cryogelation of molecularly imprinted nanoparticles: A macroporous structure as affinity chromatography column for removal of beta-blockers from complex samples.*J. Chromatogr. A* 2013, *1274*, 6-12.

(62) Chong, Y. K.; Le, T. P. T.; Moad, G.; Rizzardo, E.; Thang, S. H. A more versatile route to block copolymers and other polymers of complex architecture by living radical polymerization: The RAFT process.*Macromolecules* 1999, *32*, 2071-2074.

(63) Mayadunne, R. T. A.; Rizzardo, E.; Chiefari, J.; Chong, Y. K.; Moad, G.; Thang, S. H. Living radical polymerization with reversible addition-fragmentation chain transfer (RAFT polymerization) using dithiocarbamates as chain transfer agents.*Macromolecules* 1999, *32*, 6977-6980.

(64) Pan, G.; Zhang, Y.; Ma, Y.; Li, C.; Zhang, H. Efficient One-Pot Synthesis of Water-Compatible Molecularly Imprinted Polymer Microspheres by Facile RAFT Precipitation Polymerization.*Angew. Chem. Int. Ed.* 2011, *50*, 11731-11734.

(65) Titirici, M.-M.; Sellergren, B. Thin Molecularly Imprinted Polymer Films via Reversible Addition-Fragmentation Chain Transfer Polymerization.*Chem. Mater.* 2006, *18*, 1773-1779.

(66) Zhou, T. C.; Jorgensen, L.; Mattebjerg, M. A.; Chronakis, I. S.; Ye, L. Molecularly imprinted polymer beads for nicotine recognition prepared by RAFT precipitation polymerization: a step forward towards multi-functionalities.*R. Soc. Chem. Adv*. 2014, *4*, 30292-30299.

(67) Gibson, M. I.; Fröhlich, E.; Klok, H. A. Postpolymerization modification of Poly(Pentafluorophenyl methacrylate): Synthesis of a diverse water-soluble polymer library.*J. Polym. Sci., Part A: Polym. Chem.* 2009, *47*, 4332-4345.

(68) Haupt, K.; Mayes, A. G.; Mosbach, K. Herbicide Assay Using an Imprinted Polymer-Based System Analogous to Competitive Fluoroimmunoassays.*Anal. Chem.* 1998, *70*, 3936-3939.

(69) Levi, R.; McNiven, S.; Piletsky, S. A.; Cheong, S. H.; Yano, K.; Karube, I. Optical detection of chloramphenicol using molecularly imprinted polymers.*Anal. Chem.* 1997, *69*, 2017-2021.

(70) Chow, C.-F.; Lam, M. H. W.; Leung, M. K. P. Fluorescent sensing of homocysteine by molecular imprinting.*Anal. Chim. Acta* 2002, *466*, 17-30.

(71) Haupt, K.; Noworyta, K.; Kutner, W. Imprinted polymer-based enantioselective acoustic sensor using a quartz crystal microbalance.*Anal. Commun.* 1999, *36*, 391-393.

(72) Kriz, D.; Ramström, O.; Svensson, A.; Mosbach, K. Introducing biomimetic sensors based on molecularly imprinted polymers as recognition elements.*Anal. Chem.* 1995, *67*, 2142-2144.

(73) Wackerlig, J.; Lieberzeit, P. A. Molecularly imprinted polymer nanoparticles in chemical sensing – Synthesis, characterisation and application.*Sens. Actuator B-Chem.* 2015, *207*, 144-157.

(74) Lotierzo, M.; Henry, O. Y. F.; Piletsky, S.; Tothill, I.; Cullen, D.; Kania, M.; Hock, B.; Turner, A. P. F. Surface plasmon resonance sensor for domoic acid based on grafted imprinted polymer.*Biosens. Bioelectron.* 2004, *20*, 145-152.

(75) Ye, L.; Surugiu, I.; Haupt, K. Scintillation proximity assay using molecularly imprinted microspheres.*Anal. Chem.* 2002, *74*, 959-964.

(76) Reimhult, K.; Yoshimatsu, K.; Risveden, K.; Chen, S.; Ye, L.; Krozer, A. Characterization of QCM sensor surfaces coated with molecularly imprinted nanoparticles.*Biosens. Bioelectron.* 2008, *23*, 1908-1914.

(77) Panasyuk-Delaney, T.; Mirsky, V. M.; Wolfbeis, O. S. Capacitive Creatinine Sensor Based on a Photografted Molecularly Imprinted Polymer.*Electroanalysis* 2002, *14*, 221-224.

(78) Piacham, T.; Josell, A.; Arwin, H.; Prachayasittikul, V.; Ye, L. Molecularly imprinted polymer thin films on quartz crystal microbalance using a surface bound photo-radical initiator.*Anal. Chim. Acta* 2005, *536*, 191-196.

(79) Piletsky, S. A.; Piletska, E. V.; Chen, B.; Karim, K.; Weston, D.; Barrett, G.; Lowe, P.; Turner, A. P. F. Chemical grafting of molecularly imprinted homopolymers to the surface of microplates. Application of artificial adrenergic receptor in enzyme-linked assay for β-agonists determination.*Anal. Chem*. 2000, *72*, 4381-4385.

(80) Zourob, M. *Recognition receptors in biosensors*, 2010, p 1-863.

(81) Canfarotta, F.; Whitcombe, M. J.; Piletsky, S. A. Polymeric nanoparticles for optical sensing.*Biotechnol. Adv.* 2013, *31*, 1585-1599.

(82) Henry, O. Y. F.; Cullen, D. C.; Piletsky, S. A. Optical interrogation of molecularly imprinted polymers and development of MIP sensors: A review.*Anal. Bioanal. Chem*. 2005, *382*, 947-956.

(83) Kugimiya, A.; Takeuchi, T. Surface plasmon resonance sensor using molecularly imprinted polymer for detection of sialic acid.*Biosens. Bioelectron.* 2001, *16*, 1059-1062.

(84) Li, P.; Huang, Y.; Hu, J.; Yuan, C.; Lin, B. Surface plasmon resonance studies on molecular imprinting.*Sensors-Basel* 2002, *2*, 35-40.

(85) Surugiu, I.; Danielsson, B.; Ye, L.; Mosbach, K.; Haupt, K. Chemiluminescence imaging ELISA using an imprinted polymer as the recognition element instead of an antibody.*Anal. Chem.* 2001, *73*, 487-491.

(86) Moskovits, M. Surface-enhanced Raman spectroscopy: a brief retrospective.*J. Raman Spectrosc*. 2005, *36*, 485-496.

(87) Kostrewa, S.; Emgenbroich, M.; Klockow, D.; Wulff, G. Surface-enhanced Raman scattering on molecularly imprinted polymers in water.*Macromol. Chem. Phys.* 2003, *204*, 481-487.

(88) Chang, L.; Wu, S.; Chen, S.; Li, X. Preparation of graphene oxide-molecularly imprinted polymer composites via atom transfer radical polymerization.*J. Mater. Sci.* 2011, *46*, 2024-2029.

(89) Guo, Z.; Chen, L.; Lv, H.; Yu, Z.; Zhao, B. Magnetic imprinted surface enhanced Raman scattering based ultrasensitive detection of ciprofloxacin from a mixed sample.*Anal. Methods-Uk* 2014, *6*, 1627-1632.

(90) Chang, L.; Ding, Y.; Li, X. Surface molecular imprinting onto silver microspheres for surface enhanc24 June 2013ed Raman scattering applications.*Biosens. Bioelectron.* 2013, *50*, 106-110.

(91) Xue, J.-Q.; Li, D.-W.; Qu, L.-L.; Long, Y.-T. Surface-imprinted core–shell Au nanoparticles for selective detection of bisphenol A based on surface-enhanced Raman scattering.*Anal. Chim. Acta* 2013, *777*, 57-62.

(92) Zhang, Z.; Zhang, S.; Lin, M. DNA-embedded Au-Ag core-shell nanoparticles assembled on silicon slides as a reliable SERS substrate.*The Analyst* 2014, *139*, 2207-2213.

(93) Bompart, M.; Gheber, L. A.; De Wilde, Y.; Haupt, K. Direct detection of analyte binding to single molecularly imprinted polymer particles by confocal Raman spectroscopy.*Biosens. Bioelectron.* 2009, *25*, 568-571.

(94) Ignat, T.; Kleps, I.; Miu, M.; Craciunoiu, F.; Bragaru, A.; Simion, M. In *Proceedings of the International Semiconductor Conference, CAS*, 2008, pp 197-200.

(95) Ignat, T.; Munoz, R.; Irina, K.; Obieta, I.; Mihaela, M.; Simion, M.; Iovu, M. Nanostructured Au/Si substrate for organic molecule SERS detection.*Superlattices Microstruct.* 2009, *46*, 451-460.

(96) Kantarovich, K.; Tsarfati, I.; Gheber, L. A.; Haupt, K.; Bar, I. Writing droplets of molecularly imprinted polymers by nano fountain pen and detecting their molecular interactions by surface-enhanced Raman scattering.*Anal. Chem.* 2009, *81*, 5686-5690.

(97) Kamra, T.; Zhou, T.; Montelius, L.; Schnadt, J.; Ye, L. Implementation of Molecularly Imprinted Polymer Beads for Surface Enhanced Raman Detection.*Anal. Chem.*2015.

(98) Perney, N. M. B.; Baumberg, J. J.; Zoorob, M. E.; Charlton, M. D. B.; Mahnkopf, S.; Netti, C. M. Tuning localized plasmons in nanostructured substrates for surface- enhanced Raman scattering.*Opt. Express* 2006, *14*, 847-857.

(99) Hertz, H. Ueber einen Einfluss des ultravioletten Lichtes auf die electrische Entladung.*Ann. Phys. (Berlin)* 1887, *267*, 983-1000.

(100) Einstein, A. Generation and conversion of light with regard to a heuristic point of view.*Ann. Phys. (Berlin)* 1905, *17*, 132-148.

(101) Jenkin, J. G.; Leckey, R. C. G.; Liesegang, J. The development of x-ray photoelectron spectroscopy: 1900–1960.*J. Electron. Spectrosc. Relat. Phenom.* 1977, *12*, 1-35.

(102) Fadley, C. S. Atomic-level characterization of materials with core- and valence-level photoemission: Basic phenomena and future directions.*Surf. Interface Anal.* 2008, *40*, 1579-1605.

(103) Hüfner, S. *Photoelectron spectroscopy : Principles and Applications*, 3rd ed.; Springer, 2003.

(104) Andersen, J. N.; Hennig, D.; Lundgren, E.; Methfessel, M.; Nyholm, R.; Scheffler, M. Surface core-level shifts of some 4d-metal single-crystal surfaces: Experiments and ab initio calculations.*Phys. Rev. B* 1994, *50*, 17525-17533.

(105) Jacobs, V. L.; Behar, E.; Rozsnyai, B. F. Autoionization phenomena in dense photoionized plasmas.*J. Quant. Spectrosc. Radiat. Transfer* 2001, *71*, 397-416.

(106) Suga, S.; Sekiyama, A. In *Springer Series in Optical Sciences*, 2014, pp 1-396.

(107) Cooper, J. W. Photoionization from outer atomic subshells. a model study.*Phys. Rev.* 1962, *128*, 681-693.

(108) Cooper, J. W.; Kolbenstvedt, H. Differential energy and angular cross sections for ionization by several-hundred-keV electrons: Theory and comparison with experiment.*Phys. Rev. A* 1972, *5*, 677-687.

(109) Egelhoff Jr, W. F. Core-level binding-energy shifts at surfaces and in solids.*Surf. Sci. Rep.* 1987, *6*, 253-415.

(110) Spanjaard, D.; Guillot, C.; Desjonquères, M.-C.; Tréglia, G.; Lecante, J. Surface core level spectroscopy of transition metals: A new tool for the determination of their surface structure.*Surf. Sci. Rep.* 1985, *5*, 1-85.

(111) Tanuma, S.; Powell, C. J.; Penn, D. R. Calculations of electron inelastic mean free paths. IX. Data for 41 elemental solids over the 50 eV to 30 keV range.*Surf. Interface Anal.* 2011, *43*, 689-713.

(112) Seah, M. P.; Dench, W. A. Quantitative electron spectroscopy of surfaces: A standard database for electron inelastic mean free paths in solids.*Surf. Interface Anal.* 1979, *1*, 2-11.

(113) Fischer, H.; Svagera, R.; Ebel, H.; Ebel, M. F.; Schoßmann, B. Depth profiling by ARXPS in surface analysis.*J. Anal. Chem.* 1995, *353*, 473-477.

(114) Nyholm, R.; Andersen, J. N.; Johansson, U.; Jensen, B. N.; Lindau, I. Beamline I311 at MAX-LAB: A VUV/soft X-ray undulator beamline for high resolution electron spectroscopy.*Nucl. Instrum. Methods Phys. Res., Sect. A* 2001, *467-468*, 520-524.

(115) Schnadt, J.; Knudsen, J.; Andersen, J. N.; Siegbahn, H.; Pietzsch, A.; Hennies, F.; Johansson, N.; Mårtensson, N.; Öhrwall, G.; Bahr, S.; Mähl, S.; Schaff, O. The new ambient-pressure X-ray photoelectron spectroscopy instrument at MAX-lab.*J. Synchrotron Radiat.* 2012, *19*, 701-704.

(116) Koenig, M. F.; Grant, J. T. Deconvolution in X-ray photoelectron spectroscopy.*J. Electron. Spectrosc. Relat. Phenom.* 1984, *33*, 9-22.

(117) Shirley, D. A. High-resolution x-ray photoemission spectrum of the valence bands of gold.*Phys. Rev. B* 1972, *5*, 4709-4714.

(118) Kobayashi, H.; Yamashita, Y.; Namba, K.; Todokoro, Y. A new method for the growth of silicon oxide layers below 300 degrees C by use of catalytic activity of platinum overlayers.*Appl. Surf. Sci*. 1997, *108*, 433-438.

(119) Himpsel, F. J.; Heimann, P.; Chiang, T. C.; Eastman, D. E. Geometry-dependent Si(2p) surface core-level excitations for Si(111) and Si(100) surfaces.*Phys. Rev. Lett*. 1980, *45*, 1112-1115.

(120) Heimann, P.; van der Veen, J. F.; Eastman, D. E. Structure-dependent surface core level shifts for the Au(111), (100), and (110) surfaces.*Solid State Commun.* 1981, *38*, 595-598.

(121) Bhagavantam, S. *Chandrasekhara Venkata Raman. 1888-1970*, 1971; Vol. 17, p 564-592.

(122) Fleischmann, M.; Hendra, P. J.; Mcquilla.Aj. Raman-Spectra of Pyridine Adsorbed at a Silver Electrode.*Chem. Phys. Lett*. 1974, *26*, 163-166.

(123) Schlucker, S. Surface-Enhanced Raman Spectroscopy: Concepts and Chemical Applications.*Angew. Chem. Int. Ed.* 2014, *53*, 4756-4795.

(124) Garrell, R. L. Surface-enhanced Raman spectroscopy.*Anal. Chem.* 1989, *61*, 401 A-411 A.

(125) Kambhampati, P.; Child, C. M.; Foster, M. C.; Campion, A. On the chemical mechanism of surface enhanced Raman scattering: Experiment and theory.*J. Chem. Phys*. 1998, *108*, 5013-5026.

(126) Jiang, X.; Campion, A. Chemical effects in surface-enhanced raman scattering: pyridine chemisorbed on silver adatoms on Rh (100).*Chem. Phys. Lett.* 1987, *140*, 95-100.

(127) Xu, H. X.; Aizpurua, J.; Kall, M.; Apell, P. Electromagnetic contributions to single-molecule sensitivity in surface-enhanced Raman scattering.*Phys Rev E* 2000, *62*, 4318-4324.

(128) Garrell, R. L.; Beer, K. D. Surface-enhanced Raman spectroscopy as a probe of macromolecules.*Spectrochim. Acta B* 1988, *43*, 617-628.

(129) Moskovits, M. Surface-Enhanced Spectroscopy.*Rev. Mod. Phys*. 1985, *57*, 783-826.

(130) Aroca, R. F.; Alvarez-Puebla, R. A.; Pieczonka, N.; Sanchez-Cortez, S.; Garcia-Ramos, J. V. Surface-enhanced Raman scattering on colloidal nanostructures.*Adv. Colloid Interface Sci.* 2005, *116*, 45-61.

(131) Brown, R. J. C.; Milton, M. J. T. Nanostructures and nanostructured substrates for surface-enhanced Raman scattering (SERS).*J. Raman Spectrosc.* 2008, *39*, 1313-1326.

(132) Zhang, X. Y.; Zhao, J.; Whitney, A. V.; Elam, J. W.; Van Duyne, R. P. Ultrastable substrates for surface-enhanced Raman spectroscopy: Al2O3 overlayers fabricated by atomic layer deposition yield improved anthrax biomarker detection.*J. Am. Chem. Soc*. 2006, *128*, 10304-10309.

(133) Binnig, G.; Quate, C. F.; Gerber, C. Atomic Force Microscope.*Phys. Rev. Lett*. 1986, *56*, 930-933.

(134) Bhushan, B.; Marti, O. Scanning Probe Microscopy - Principle of Operation, Instrumentation, and Probes.*Nanotribology and Nanomechanics: Measurement Techniques and Nanomechanics, Vol 1* 2011, 37-110.

(135) von Ardenne, M. Das Elektronen-Rastermikroskop.*Z Phys* 1938, *109*, 553-572.

(136) McMullan, D. Scanning electron microscopy 1928–1965.*Scanning* 1995, *17*, 175-185.

(137) Kemmnitz, G.; Knoll, M.; Walcher, W. Investigation by the electron concentration of concave incandescent cathode surfaces with the electron microscope.*Z Phys* 1935, *96*, 612-619.

(138) Knoll, M. Charge potential and secondary emissions of electron irradiated bodies.*Phys Z* 1935, *36*, 861-869.

(139) The spectroscopic electron microscope. (cited february 20, 2015) http://www.eng.nus.edu.sg/EResnews/0502/rd/rd_7.html 2005).

(140) Wheatley, J. B.; Schmidt Jr, D. E. Salt-induced immobilization of affinity ligands onto epoxide-activated supports.*Journal of Chromatography A* 1999, *849*, 1-12.

(141) Ulman, A. Formation and structure of self-assembled monolayers.*Chemical reviews* 1996, *96*, 1533-1554.

(142) Love, J. C.; Estroff, L. A.; Kriebel, J. K.; Nuzzo, R. G.; Whitesides, G. M. Self-assembled monolayers of thiolates on metals as a form of nanotechnology.*Chemical reviews* 2005, *105*, 1103-1169.

(143) Hansen, R. W. C.; Wolske, J.; Takacs, P. Z. UV/ozone cleaning of a replica grating.*Nuclear Inst. and Methods in Physics Research, A* 1994, *347*, 254-257.

(144) Mak, W. C.; Georgieva, R.; Renneberg, R.; Bäumler, H. Protein particles formed by protein activation and spontaneous self-assembly.*Adv. Funct. Mater.* 2010, *20*, 4139-4144.

(145) Staros, J. V.; Wright, R. W.; Swingle, D. M. Enhancement by N-hydroxysulfosuccinimide of water-soluble carbodiimide-mediated coupling reactions.*Anal. Biochem.* 1986, *156*, 220-222.

(146) Kobayashi, S.; Tokunoh, M.; Saegusa, T.; Mashio, F. Poly(allylamine). Chelating properties and resins for uranium recovery from seawater.*Macromolecules* 1985, *18*, 2357-2361.

(147) Parker, R. E.; Isaacs, N. S. Mechanisms Of Epoxide Reactions.*Chem. Rev.* 1959, *59*, 737-799.

(148) Chen, W.; McCarthy, T. J. Layer-by-Layer Deposition: A Tool for Polymer Surface Modification.*Macromolecules* 1997, *30*, 78-86.

(149) Xue, Y. R.; Li, X.; Li, H. B.; Zhang, W. K. Quantifying thiol-gold interactions towards the efficient strength control.*Nat. Commun.* 2014, *5*, 1-9.

(150) Levene, C.; Correa, E.; Blanch, E. W.; Goodacre, R. Enhancing surface enhanced Raman scattering (SERS) detection of propranolol with multiobjective evolutionary optimization.*Anal. Chem.* 2012, *84*, 7899-7905.

(151) Sun, C. H.; Wang, M. L.; Feng, Q.; Liu, W.; Xu, C. X. Surface-enhanced Raman scattering (SERS) study on Rhodamine B adsorbed on different substrates.*Russ. J. Phys. Chem.* 2015, *89*, 291-296.

(152) Renkecz, T.; Ceolin, G.; Horváth, V. Selective solid phase extraction of propranolol on multiwell membrane filter plates modified with molecularly imprinted polymer.*The Analyst* 2011, *136*, 2175-2182.

(153) Boonjob, W.; Sklenářová, H.; Lara, F. J.; García-Campaña, A. M.; Solich, P. Retention and selectivity of basic drugs on solid-phase extraction sorbents: Application to direct determination of β-blockers in urine.*Anal. Bioanal. Chem.* 2014, *406*, 4207-4215.

(154) Álvarez, A.; Costa, J. M.; Pereiro, R.; Sanz-Medel, A. Reusable phosphorescent probes based on molecularly imprinted polymers for the determination of propranolol in urine.*Sens. Actuators B-Chem.* 2012, *168*, 370-375.

(155) Premasiri, W. R.; Clarke, R. H.; Womble, M. E. Urine analysis by laser Raman spectroscopy.*Lasers Surg. Med.* 2001, *28*, 330-334.